

MODELLING WIRELESS POWER TRANSFER USING AN ARRAY OF TESLA COILS

by

CASEY THOMAS PIERSON

University of Central Oklahoma

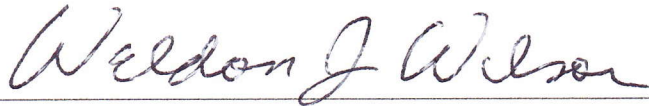
Edmond, Oklahoma

2017

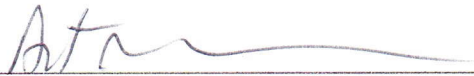
Submitted to the Faculty of the
Graduate College of the
University of Central Oklahoma
in partial fulfillment of
the requirements for
the Degree of
MASTER OF SCIENCE
July, 2017

MODELLING WIRELESS POWER TRANSFER
USING AN ARRAY OF TESLA COILS

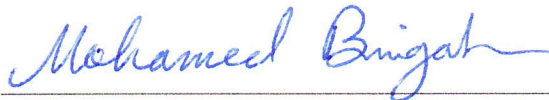
Thesis approved:



Dr. Weldon J. Wilson, Chair



Dr. Abdellah Ait Moussa



Dr. Mohamed Bingabr

Acknowledgements

I'd like to thank Dr. Wilson for his insights, sagely advice, and wicked humor to keep me sane. I'd also like to thank Dr. Ait Moussa for answering my very specific inquiries, sometimes with a raised eyebrow, and Dr. Bingabr for dealing with my incisive questioning with dignity and patience. My gratitude goes out to Derek Marzolf, Byron Okine, Cagatay Mital, and Andrew Matthews for their hard work and time, and to the UCO Department of Engineering Physics for making this project possible.

For all of my incredible family, friends, and colleagues, who helped me keep my head up, my mind working, and my hands writing, and my lovely wife, who somehow was able to tolerate my incessant rambling.

“It is a mistake to think you can solve any major problems just with potatoes.”

Douglas Adams

Name: CASEY THOMAS PIERSON

Date: JULY, 2017

Title of Study: MODELLING WIRELESS POWER TRANSFER USING AN ARRAY OF TESLA COILS

Major Field: ENGINEERING PHYSICS/PHYSICS

Abstract: Wireless power transmission, or WPT, is a well-demonstrated property in electrical science and physics. Coil-and-wave transmission (CWT) consists of two Tesla coils, one powered by a controlled voltage source v_{src} and one connected across a generic load Z_0 , at a mid- to long range distance apart with spherical capacitors at each of their top loads. The literature on the different methods of WPT varies widely, but research of CWT is sparse, lacking especially in the area of computer simulation. Recently, a physical experiment was conducted by Marzolf et al. in [1], and yielded surprising resonant frequencies in the high frequency range. The goal of this research is to answer the question of whether these resonant frequencies originate in unexplained field effects or in non-ideal circuit behavior, and establish a formal model to indicate at what frequencies the resonant peaks occur as a first approximation. By carefully constructing a simulation of the most geometrically simple, power efficient design in the work of Marzolf et al. using the scientific software Octave, we investigate these frequencies computationally: first, an ideal scenario that has no flux leakage or exterior losses is modelled mathematically and simulated, and then, a non-ideal scenario that accounts for losses in the coils and surroundings is modelled mathematically and simulated. Both models utilize a simple formula for spherical capacitance for the top loads. After running these simulations through detailed sampling up to 4 MHz, the ideal model could not account for the resonant peaks, while the non-ideal model indicated the resonant peaks near the exact frequency ranges that were observed in [1]. An unexpected characteristic of these results was that coupling coefficients between the coils of the transmitter and receiver played a noticeable part in the indication of resonant peaks. This demonstrates that unknown field effects are not the primary driver of resonance in the ideal or non-ideal construction, and raises intriguing questions about the circuit design's relationship with resonance in the locality about the coils.

Contents

Signatures and Approval	i
Acknowledgements	ii
Abstract	iii
List of Figures	vii
List of Tables	viii
Abbreviations	ix
Physical Constants	x
Symbols	xi
1 Introduction	1
1.1 Coil-and-Wave Transmission (CWT)	1
1.1.1 Overview of the Mechanism	2
1.1.2 Advantages and Disadvantages	4
1.2 The Method of Simulating CWT	4
2 The Status of Literature on WPT	6
2.1 The Dearth of CWT Literature	6
2.2 A Plethora of SRMI and LRMI Special Cases	7
2.3 Questions of Quality and Validity	7
3 Modelling CWT Using an Ideal Configuration	8
3.1 Setup	8
3.2 Formulation	9
3.2.1 Circuit Analysis and Equivalence	9
3.2.2 Model Coil Equivalence Assumptions	11
3.2.3 Generic Formulations of Capacitor Field Interactions	11
3.3 End Computation	13

4	Modelling CWT Using a Non-Ideal Configuration	15
4.1	Setup	15
4.2	Formulation	17
4.2.1	Circuit Analysis and Equivalence	17
4.2.2	Experimental Properties and Eccentric Physical Effects	23
4.2.2.1	Equivalence Parameters	23
4.2.2.2	Inductance and Geometry of Capacitors	23
4.2.2.3	Resistance - Skin Effect, Proximity Effect, and Material Properties	25
4.2.3	Capacitor Field Interactions	27
4.3	End Computation	28
4.3.1	Symbolic Computational Forms	28
4.3.2	Component Numerical Information	29
5	Simulation Results	31
5.1	Ideal Model	31
5.2	Non-ideal Model	31
6	Conclusions	38
A	Formulas	40
B	Code	45
B.1	Ideal Simulation	45
B.2	Non-ideal Simulation	46
C	Data and Figures for Empirical Formulas	51
D	Detailed Numerical Calculations	54
	Bibliography	57

List of Figures

1.1	Ideal mechanism of CWT transfer.	2
3.1	Ideal mechanism of CWT transfer with parasitic capacitance.	8
3.2	Ideal mechanism of CWT transfer with loop currents.	10
4.1	Experimental setup with representative and physical components	15
4.2	Experimental setup with series combined impedances	18
4.3	Experimental setup with combined impedances along medium resistance and medium leakage	18
4.4	Setup for simplified analysis on both transmitter and receiver circuits. . .	20
5.1	Lab results of physical study	33
5.2	Ideal simulation results	34
5.3	Non-ideal simulation results at fixed k values	35
5.4	Non-ideal simulation results with free coupling k	36
5.5	Phase as a function of free coupling k and frequency ω	37
C.1	American Wire Gauge (AWG) Equivalent Metric Measurements	51
C.2	Medhurst interpolation	53

List of Tables

C.1 Table of Medhurst Values for Self-Capacitance	52
---	----

Abbreviations

WPT	Wireless power transmission
CWT	Coil-and-wave transmission
SRMI	Short range magnetic induction
LRMI	Long range magnetic induction
LPRF	Low power radio frequency
LED	Light emitting diode

Physical Constants

Speed of light	c	$=$	$2.997\,924\,58 \times 10^8 \text{ m} \cdot \text{s}^{-1}$ (exact)
Vacuum permeability	μ_0	$=$	$4\pi \times 10^{-7} \text{ V} \cdot \text{s} \cdot \text{A}^{-1} \cdot \text{m}^{-1}$
		\approx	$1.256\,637\,061\,4 \times 10^{-7} \text{ V} \cdot \text{s} \cdot \text{A}^{-1} \cdot \text{m}^{-1}$
Vacuum permittivity	ϵ_0	$=$	$\mu_0^{-1} c^{-2}$
		\approx	$8.854\,187\,817\,620 \times 10^{-12} \text{ C} \cdot \text{V}^{-1} \cdot \text{m}^{-1}$
Electrical resistivity of air	ρ_a	\in	$[1.30, 3.30] \times 10^{14} \text{ } \Omega \cdot \text{m}$
Imaginary component (phasor form)	j	$=$	$\sqrt{-1}$

Symbols

n	generic positive integer	(unitless)
N	generic positive integer total	(unitless)
x	generic distance	m
v	generic velocity	$\text{m} \cdot \text{s}^{-1}$
U	energy	J
\mathcal{U}	energy density per dimension n	$\text{J} \cdot \text{m}^{-n}$
F	force	N
\mathcal{F}	force density per dimension n	$\text{N} \cdot \text{m}^{-n}$
q	charge (discrete)	C
dq	charge (infinitesimal)	C (infinitesimal)
Q	total charge	C
V	voltage	V ($\text{J} \cdot \text{C}^{-1}$)
\mathcal{E}	electromotive force (EMF)	V
I	current	A ($\text{C} \cdot \text{s}^{-1}$)
dI	current (infinitesimal)	A (infinitesimal)
R	resistance	Ω
Z	impedance	Ω
P	power	W ($\text{J} \cdot \text{s}^{-1}$)
\mathcal{P}	power density per dimension n	$\text{W} \cdot \text{m}^{-n}$
E	electric field	$\text{V} \cdot \text{m}^{-1}$ ($\text{N} \cdot \text{C}^{-1}$)
dE	electric field (infinitesimal)	$\text{V} \cdot \text{m}^{-1}$ (infinitesimal)
D	electric displacement field	$\text{C} \cdot \text{m}^{-2}$
B	magnetic field	$\text{T} \cdot \text{m}^{-1}$
dB	magnetic field (infinitesimal)	$\text{T} \cdot \text{m}^{-1}$ (infinitesimal)
H	magnetizing field	$\text{A} \cdot \text{m}^{-1}$
L	inductance	H

M	mutual inductance	H
C	capacitance	F ($\text{C} \cdot \text{V}^{-1}$)
λ	linear charge density	$\text{C} \cdot \text{m}^{-1}$
σ	surface charge density	$\text{C} \cdot \text{m}^{-2}$
ρ	volume charge density	$\text{C} \cdot \text{m}^{-3}$
$d\lambda$	linear charge density (infinitesimal)	$\text{C} \cdot \text{m}^{-1}$ (infinitesimal)
$d\sigma$	surface charge density (infinitesimal)	$\text{C} \cdot \text{m}^{-2}$ (infinitesimal)
$d\rho$	volume charge density (infinitesimal)	$\text{C} \cdot \text{m}^{-3}$ (infinitesimal)
ϕ	scalar potential	V
\vec{A}	vector potential (contextual)	$\text{V} \cdot \text{s} \cdot \text{m}^{-1}$
\vec{A}	area/surface area normal vector (contextual)	m^2
Φ_B	magnetic flux	$\text{T} \cdot \text{m}^2$

Chapter 1

Introduction

The validity of wireless power transfer (WPT) is a widely, and sometimes hotly, debated topic. Most researchers agree that theoretical methods are available, but the practicality of these methods is subject to intense scrutiny and viewed as near-impossible for everyday far-field applications [2]. Thanks to both a revival of interest by large-value companies (and, speculatively, by the spread of media detailing Tesla coils in action), a new band of scientists, engineers, and erudite makers have attempted to pursue WPT at a larger scale. The goal of this chapter is to present a technical overview of two subjects of interest: first, a mechanical examination of coil-and-wave transmission (CWT), which utilizes a powered Tesla coil to transmit to a receiving Tesla coil; second, a broad analysis of other successful methods of far field WPT, including magnetic induction.

1.1 Coil-and-Wave Transmission (CWT)

CWT takes advantage of two modified Tesla coils, one acting as a transmitter and the other acting as a receiver. In this setup, the transmitting Tesla coil is powered by an AC power source, while the receiving Tesla coil is connected across a load Z_0 . Theoretical explorations of this do exist, but are thin. Additionally, such articles are also few and far between. As a result, much of this work is based on data collected from a design group at UCO [1]. From experiments conducted by Marzolf et al., however, the efficiency of power transferred across empty space is certainly low, both with respect to toroidal top geometry and spherical top geometry. (Note that mixed geometries have not been attempted using this method; this will be revisited and explored in a later section, and critically evaluated in a later chapter.)

1.1.1 Overview of the Mechanism

Figure 1.1 illustrates the ideal mechanism for the CWT system. An AC voltage source of known quality, v_{src} , is attached across a primary cylindrical coil of few turns, moderate wire radius, and large coil diameter. This is coupled to a secondary coil with significantly more turns, smaller wire radius, and smaller coil diameter. The coupling forms a transformer, which steps v_{src} up by a large turn ratio $(N_p/N_s)^{-1}$, where N_p is the number of turns in the primary coil and N_s is the number of turns in the secondary coil. This stepped up voltage is then run across a spherical conductor, and generates an alternating electric field \vec{E} , creating time-dependent spherical waves. On the receiving end, a spherical conductor receives this \vec{E} field and subsequently generates its own current density. This leads to a voltage, v_2 , which is then stepped down through a symmetric transformer by the same turn ratio N_p/N_s , resulting in a stepped-down voltage v_{out} . A load Z_0 is connected across v_{out} , and is used for readings.

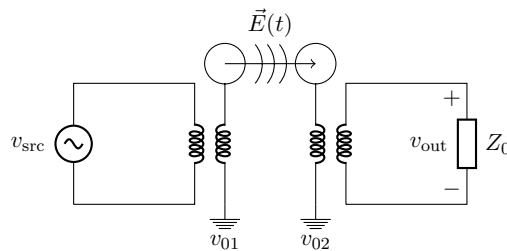


FIGURE 1.1: Ideal mechanism of CWT transfer.

There are several plausible ways to go about modelling the transmission of energy between the two spheres, each with their own advantages and disadvantages. A description of each is laid out below.

1. *Joint capacitors with a resistor*: The two spheres may be modelled as two capacitors, C_t and C_r , in series with a resistor between them. This resistor would have the characteristics of air, and thus take a massive resistivity on the order of $10^{16} \Omega\text{m}$ over a distance l and an approximate cross-sectional area A . There exists an obvious downside to this approach: modelling the resistor depends heavily on the status of the field through the air gap, and as such defies some conventional evaluations. Further, as the input current will vary with time, field lines may rectify and change directions between the two capacitors, and the resistor model could vary in cross-sectional area, thus changing resistance over time as

well. Some traditional circuit theory can certainly accommodate this, but continued use of simple assumptions of time-varying resistance would be better modelled through a battery of tests or simulations of time-dependent geometries for the air gap resistor, which lies beyond the scope of this work.

2. *Capacitance of two conducting separate spheres:* By taking one of Maxwell's lesser-used formulas as presented in [3] and [4], the capacitance between two spheres of equal radius r at a certain distance l apart may be calculated to extremely close precision as follows:

$$C_s = 2\pi\epsilon r \sum_{n=1}^{\infty} \frac{\sinh \left[\ln(D + \sqrt{D^2 - 1}) \right]}{\sinh \left[n \ln(D + \sqrt{D^2 - 1}) \right]} \approx 2\pi\epsilon r \left[\ln 2 + \gamma - \frac{1}{2} \ln(2D - 2) \right].$$

Above, γ is the Euler constant ($\gamma \approx 0.5772156649$), and $D = l/2r > 1$. There may exist some discrepancies in this calculation due to the spheres' proximity with the ground; consequently, this model requires basic reformulation of the circuit such that the two spheres are in fact one capacitor, C_s , acting in series with both the transmitter and receiver circuits, and extended to a height such that capacitance with the ground is no longer an issue. One incredible benefit of this method is that voltage calculations are coerced into more intuitive forms, as the circuits are no longer separated mathematically by an air gap except in the calculation of the capacitance. However, a notable shortcoming is that the included formula claims only to work for a short separation l between the two spheres. As before, an interesting discussion may be had over such assumptions and calculations, but the setup of a CWT system may not necessarily accommodate the close separation restriction on l .

3. *Electric field between two conducting spheres of shared characteristics:* Similar to method (1), the two spheres are modelled as two capacitors, C_t and C_r , where C_t is the transmitting capacitor and C_r is the receiving capacitor. The electric field generated from the transmitting capacitor is estimated using the following formula for the capacitance of a conducting isolated sphere:

$$C_t = 4\pi\epsilon r.$$

This same formula is re-evaluated at the receiving sphere after adequate transmission time; so, since the radius of each sphere is the same, $C_t = C_r$. Under this paradigm, the circuit does not require reformulation, but careful analysis must happen across the air gap to determine energy transfer, and subsequent voltage readings, at the receiver circuit through an electric field. Although similar to modelling a capacitor of two separated spheres, utilizing the electric field between C_t and C_r would allow for more segmentation in most calculations that must take place, though it should be noted that a similar reflection issue as in method (2) may occur at short heights.

Despite its shortcomings, method (3) was determined to be appropriate for ideal and non-ideal circuit analysis, given that treating the air gap as a resistor would lead to extraordinary mathematical difficulty, and modelling the air gap as a capacitor between two spheres yields uncertain reliability due to its limitation on separation distance.

1.1.2 Advantages and Disadvantages

Advantages that are not immediately obvious manifest in this approach. Modelling CWT in this way, for example, may be extensible over distance. The future of CWT arguably hinges on its practicality over distance, so this is no small feat. Also, since selection of non-ideal properties in both the math and the code are imperative, our model contains more modularity and segmentation than one might expect, leading to additional room for modification and alternative theory should the need arise.

However, just as the advantages of this method are obfuscated, so too are its disadvantages. Non-ideal modelling of CWT from a circuit perspective is, in a word, tedious. Equivalence measures have to be taken across the transformers at each coupling, and these are somewhat approximate. Careless use under the right circumstances could result in vastly different numbers than reality shows, something we hope to mitigate with modelling these non-ideal conditions extremely carefully.

1.2 The Method of Simulating CWT

For both the ideal and non-ideal constructions, parasitic capacitance will be accounted for. The reasoning for this in the non-ideal case might be obvious, but in the ideal case, accounting for parasitic capacitance may increase the model's accuracy-to-fit, as the rough simulation and data taken in [1] accounted for this without accounting for

leakage or magnetizing inductance. As expected, the main difference that exists in the non-ideal from this is taking into account those quantities that were not in the ideal case: magnetizing inductance, leakage inductance, and material resistance.

In the construction of an ideal and non-ideal simulation, geometry and paths are kept simple for the sake of first approximation, which is yet another benefit of the third listed approach of modelling capacitance. Taking simple partial derivatives across an air gap, assuming no magnetic vector potential (again, for simplicity), evaluates electric field “throughput” via the transmitting capacitor to the receiving capacitor. Upon completion of both ideal and non-ideal models, their results and resonance patterns are compared to that found in experimental data gathered by the design group at UCO in [1]. This is how accuracy and feasibility will be determined in both cases.

It should be noted that the function embedding performed in the code utilized by the simulations is extraordinary, and would be difficult to construct without a syntax to declare anonymous, immediate functions, and pass them directly to other anonymous functions, such as that that exists in MATLAB or Octave. Despite Octave being used for this coding, syntax compatibility exists between Octave and MATLAB; as such, the code is made in such a way as to attempt to preserve this compatibility.

Chapter 2

The Status of Literature on WPT

The portrait of competing mechanisms in the first chapter of this text is heavily based on the underlying physics of each system being well-investigated. There exists no need for difficult, esoteric physics or engineering in the scope of any apparatus of concern (although extensibility will be discussed later in this work). Indeed, a wide variety of literature exists on the subject, and much of the difficulty of analysis lies in the computational demands placed on any human or machine solver. Alarming, however, very little intellectual stock is invested in CWT in published format. The reasons for this are not obvious, but one quickly notices a proliferation of WPT research that focuses almost exclusively on the varying methods of magnetic induction. Even so, much of this literature is sufficient only for extremely narrow scopes of experimentation.

2.1 The Dearth of CWT Literature

CWT applications have been examined in a cursory capacity, but have not been thoroughly investigated in recent years. As mentioned in the previous section, this is a surprising find. Reasons for this fall solely on the shoulders of efficiency and mystery, however [2], and as it stands, CWT appears to be in danger of being circumvented for magnetic resonance methods. As CWT is closely based on Tesla's approach [5], ample time has passed for modified versions of CWT to arise [6] [7]. A large mindshare exists on re-examining demonstrations of Tesla's work [8] [2] in terms of its efficiency over large distances, but rely on justifying magnetic resonance cases for good short range alternatives.

Thankfully, rigorous research into solution-finding has continued. Some of the most efficient, analytic work done on the topic of solution-finding for CWT was conducted by Liu et. al. in their incisive solutions for a retarded phase factor in an ideal case [9] [10] [11], and serves as an implicit basis for the examination of the phase factor in this work.

Simulations are used regularly to examine antennas, EM effects at far range, and EM in extreme circumstances and conditions, and seem to be a natural fit for simulating WPT. However, once again, there are seemingly few analytic examinations of CWT that exist that make use of simulation or multiphysics modelling and, once again, this remains surprising. Strangely, simulation is thoroughly used in the construction of magnetic resonance apparatus and theory, but seems to have not found strong footing in CWT methodology as of this writing.

2.2 A Plethora of SRMI and LRMI Special Cases

A large subfield of applied ODEs revolves around magnetic coupling. In the work of Christianto and Smarandache [12], numerical solutions are found for coupled magnetic systems. Meanwhile, in another work featuring Christianto [13], an exact solution is found for the same system. Several more articles and works follow this same pattern, and partake heavily in simulation to verify those results. In truth, this is a very convenient field of research to seek out, as it has multiple applications in electronics, imaging, and fabrication, but it also narrows the pool of available research for CWT somewhat further.

2.3 Questions of Quality and Validity

Questions arise about much of this research. CWT has by no means been abandoned, but what factors cause it to lose its value in the literature? Why are more simulations not being conducted? Certainly power efficiency plays a role, and a corollary to the more pessimistic reader would center on if investigation into CWT should any longer be conducted at all with the advent of strong-promising additional methods [2] [14]. Our work may very well open some doors to these questions, even though that is not its intended purpose.

Chapter 3

Modelling CWT Using an Ideal Configuration

3.1 Setup

The following diagram is based on an ideal configuration of the laboratory setup in [1]:

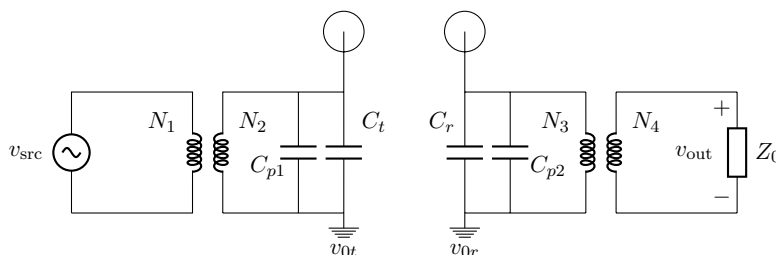


FIGURE 3.1: Ideal mechanism of CWT transfer with parasitic capacitance.

The circuit looks simple at first glance, but the air gap between the two spheres requires more examination, and is more complicated than it appears. Below, each component is described in summary.

Transformer couplings: The N_1 , N_2 coupling and the N_3 , N_4 coupling represent the first and second transformer couplings, respectively. These take the usual form where for some primary winding N_p and secondary winding N_s , a step-up comparison has that $N_s > N_p$ and a step-down configuration has that $N_p > N_s$.

Spherical capacitors: The capacitors, C , represented on the diagram by a capacitor symbol wrapped in a circle, symbolize the spherical capacitors being used as a transmitter-receiver system. Although these look to be “dangling components” similar to antenna relays, the diagram is a bit beguiling as the isolated spherical capacitors are, in fact,

connected through a complete circuit. Also, the mechanics are somewhat distinct from the behavior of an antenna relay, and the math surrounding an antenna relay system is not necessarily the most efficient methodology to rely on. Consequently, careful wave analysis is used across the air gap between C_t and C_r , and will be detailed in following sections.

Parasitic capacitance: On the circuit diagram, the parasitic capacitors, C_p , represent the stray capacitance that the secondary coil on the transmitter and the primary coil on the receiver exhibit. This effect is negligible at low frequencies, but since the scope of the simulation extends to relatively high (~ 3 MHz) frequencies, parasitic capacitance must be accounted for.

Dual grounding: A quirk of this diagram's setup is that there are two distinct "earth" grounds, v_{0_t} (for the transmitter circuit) and v_{0_r} (for the receiver circuit). This is due to the nature of the experiment being run: extremely high voltages run the risk of conducting through an insufficient ground, especially when contending with the resistivity of air, which is on the order of $10^{14} \Omega \cdot \text{m}$. It should be noted that one of the approaches investigated relies on examining resonant frequencies through the length of the ground and the coils, and as such, the distinction between these two points is even more imperative.

Load on receiver: Finally, a generic load of impedance Z_0 is included for indication of power transmission. This is the load across which v_{out} is measured. In the laboratory experiment conducted by [1], this load was an LED. A voltmeter may be attached across this load without noticeable consequence to the circuit, and is thus not diagrammed.

3.2 Formulation

3.2.1 Circuit Analysis and Equivalence

By operating with impedances, we are able to use common formulas and properties for passive circuits efficiently for this model. As expected, let

$$Z_{p1} = 1/j\omega C_{p1},$$

$$Z_{Ct} = 1/j\omega C_t,$$

$$Z_{Cr} = 1/j\omega C_r,$$

$$Z_{p2} = 1/j\omega C_{p2}.$$

Now let I_1 and I_2 be loop currents around the first and second loops in the transmitter circuit after the secondary coil, and I_3 and I_4 be loop currents around the first and second loops in the receiver circuit before the primary coil, as illustrated below:

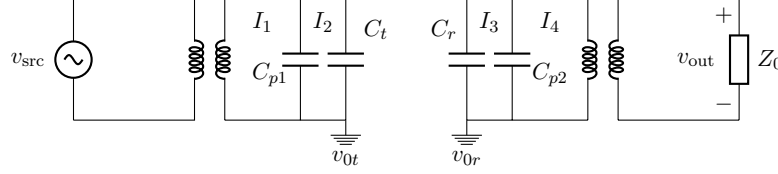


FIGURE 3.2: Ideal mechanism of CWT transfer with loop currents.

Now first by evaluating Figure 3.1 using ideal transformer equations and using KVL with loop currents, we find that

$$\left(\frac{N_2}{N_1}\right)v_{\text{src}} = v_{Ct},$$

as the voltage across the parasitic capacitor readily substitutes out. (*Note:* For convenience in the future, we will set $a_1 = N_1/N_2$ and $a_2 = N_3/N_4$.) So, since v_{src} is sinusoidal (AC) in the usual way, where

$$v_{\text{src}}(t) = V_{\text{max}} \sin(\omega t),$$

this will reflect in the relationship between the voltage across v_{Ct} :

$$v_{Ct} = \left(\frac{N_2}{N_1}\right)V_{\text{max}} \sin(\omega t).$$

Using mesh analysis, then, a basic system of equations for both the transmitter (currents I_1 and I_2) and the receiver (currents I_3 and I_4) can be set up with impedances of each circuit, as expected:

$$\left. \begin{aligned} -a_1 v_{\text{src}} + (I_1 - I_2)Z_{Cp1} &= 0 \\ -(I_1 - I_2)Z_{Cp1} + I_2 Z_{Ct} &= 0 \end{aligned} \right\} \text{Transmitter}$$

$$\left. \begin{aligned} -I_3 Z_{Cr} + (I_3 - I_4)Z_{Cp2} &= 0 \\ -(I_3 - I_4)Z_{Cp2} + a_2^2 I_4 Z_0 &= 0 \end{aligned} \right\} \text{Receiver}$$

However, we also take $I_3 Z_{Cr} = v_{Cr}$, which is treated as a constant with respect to its loop current. We then may solve for each loop current using basic algebraic means:

$$\begin{aligned} I_1 &= a_1 \frac{v_{\text{src}}}{Z_{Cp1}} \left(\frac{Z_{Cp1}}{Z_{Ct}} + 1 \right), \\ I_2 &= a_1 \frac{v_{\text{src}}}{Z_{Ct}}, \\ I_3 &= \frac{v_{Cr}}{Z_{Cp2}} \left(\frac{Z_{Cp2}}{a_2^2 Z_0} + 1 \right), \\ I_4 &= \frac{v_{Cr}}{a_2^2 Z_0}. \end{aligned}$$

The phasor of v_{out} is gained from repeated substitution:

$$v_{\text{out}} = I_4 Z_0 = \frac{v_{Cr}}{a_2^2} = \frac{I_3 Z_{Cr}}{a_2^2} = \frac{v_{Cr}}{a_2^2} \frac{Z_{Cr}}{Z_{Cp2}} \left(\frac{Z_{Cp2}}{a_2^2 Z_0} + 1 \right).$$

By writing each impedance in explicit form, then, we have

$$v_{\text{out}}(\omega) = \frac{v_{Cr}}{a_2^2} \frac{C_{p2}}{C_r} \left(1 - j \frac{1}{a_2^2 Z_0 \omega C_{p2}} \right). \quad (3.1)$$

3.2.2 Model Coil Equivalence Assumptions

For our model, we assume several important equivalence parameters. The primary coil of the transmitter has the same physical characteristics as the secondary coil of the receiver, and the secondary coil of the transmitter has the same physical characteristics as the primary coil of the receiver, such that ideal calculations fall into place. Also, the following coil counts are equivalent, and given a match variable n for convenience:

$$N_1 = N_4 = n_1$$

$$N_2 = N_3 = n_2$$

This is somewhat essential for the ideal model, as will be detailed in §3.3.

3.2.3 Generic Formulations of Capacitor Field Interactions

The key to further analysis is determining what sort of coupling the two equations have. As described in §1.1.1, the paradigm that we select will allow us first to model each

capacitor as an isolated sphere of equivalent radius r_C , such that

$$C_t = C_r = 4\pi\epsilon r_C.$$

Now, with capacitors, recall that $Q = VC$. At the transmitting capacitor, this property is useful for determining the radiative electric field \vec{E} about the sphere, and is used in the following way:

$$Q_{Ct} = v_{Ct} \cdot C_t = \left[\left(\frac{n_2}{n_1} \right) V_{max} \sin(\omega t) \right] \cdot 4\pi\epsilon r_C.$$

By describing the electric field in the usual way for a conducting sphere, such that

$$\vec{E} = \frac{Q}{4\pi\epsilon r^2} \hat{r},$$

then we have the following for an emanating electric field \vec{E} at displacement r from the transmitting sphere of charge Q_{Ct} :

$$\vec{E} = \left(\frac{n_2}{n_1} \right) \frac{r_C V_{max}}{r^2} \sin(\omega t) \hat{r}. \quad (3.2)$$

From this, we may also gather a voltage across the air gap. For an electric field, the potential ϕ about the field source is related to the electric field as

$$\vec{E} = -\nabla\phi.$$

If we assume a straight path along x between the spheres, then this is easily approximated by using the partial derivative in the x direction:

$$\begin{aligned} E &= -\frac{\partial\phi}{\partial x} \approx -\frac{\Delta V}{\Delta x} \\ \longrightarrow \Delta V &= -E\Delta x = -E\Delta r. \end{aligned}$$

So, by using this approximation and by taking the transmitting and receiving capacitors to be located at $r_t = 0$ and r_r , we have

$$v_{Cr} = v_{Ct} - \frac{n_2}{n_1} \frac{r_C V_{max}}{r_r^2} (r_r - 0) \sin(\omega t).$$

Substituting $v_{Ct} = \frac{n_2}{n_1} V_{\max} \sin(\omega t)$ in yields an explicit form for the voltage at the receiver:

$$v_{Cr} = \frac{n_2}{n_1} V_{\max} \left(1 - \frac{r_C}{r_r} \right) \sin(\omega t). \quad (3.3)$$

It bears saying that although this is an appropriate first approximation, as with the rest of the composition of the ideal model, there are certain assumptions that make our model notably more efficient in handling WPT than what may be dictated in reality. In this case, we assume a straight path r in line with an electric field generated at C_t transmitting to C_r . Although path independence lends credibility to this assumption, it is thought that some “rectification” of the electric field’s linear waves contributes to the transmission efficiency over time. Because of this, during computation, we may only safely assume these properties only after some time has passed.

3.3 End Computation

A convenient formulation can be made for v_{out} follows from equations (3.1) and (3.3) in phasor form (without $\sin \omega t$):

$$v_{\text{out}}(\omega) = \frac{V_{\max}}{a_2} \frac{C_{p2}}{C_r} \left(1 - \frac{r_C}{r_r} \right) \left(1 - j \frac{1}{a_2^2 Z_0 \omega C_{p2}} \right). \quad (3.4)$$

Each of these constants has a given value based on experimentation:

$$r_C = 0.06 \text{ m},$$

$$r_r = 1 \text{ m},$$

$$C_t = C_r = 6.673 \text{ pF},$$

$$C_{p1} = C_{p2} = 4.274 \text{ pF},$$

$$V_{\max} = 15 \text{ V},$$

$$a_2 = 100.$$

This is a detailed, idealized description of v_{out} as a function of ω , which will be simulated as such. C_{p1} and C_{p2} are expected to be the same in the ideal case, as we model them both off of the higher turned coils. We will see in the non-ideal scenario in chapter 4

that modelling parasitic capacitance for the secondary coil on the transmitter is also sufficient. Note that r_r is always in reference to $r_t = 0$.

Chapter 4

Modelling CWT Using a Non-Ideal Configuration

4.1 Setup

The following diagram is a generic, non-ideal description of the tested CWT laboratory setup:

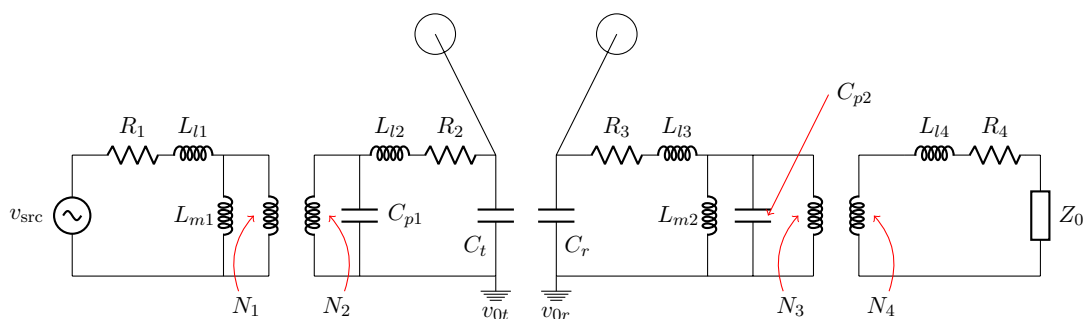


FIGURE 4.1: Experimental setup with representative and physical components

Unlike the ideal case, one must cautiously discern between physical components and additions to the circuit that are representative of losses of energy or magnetomotive-affected areas, especially across inductors that are built into the diagram. Each of these physical or representative components is discussed in detail here.

Magnetizing inductance: Inductors represented by L_m are not physical inductors, but representative of the magnetizing inductance that excites the transformer core, and is inversely proportional to the reluctance, \mathcal{R} , of the transformer core. This is described in greater detail later. The core of each of these transformers is essentially air, so this is largely minimized, though not something to be overlooked.

Leakage inductance: The L_l inductors are also not physical components; instead, they represent leakage inductance across each coil that is utilized in each transformer. These are also non-negligible, even in most idealized transformers [15].

Resistance of media: The resistors, R , built into series with the leakage inductors represent numerous resistive factors in the coils used across each transformer. Due simply to the nature of the step-up transformation that must be performed for power to be noticeably apparent from the transmitter to the receiver, these resistive factors are important to include for thoroughness in analysis, particularly due to how much of a transformation is performed at each coupling in the transformers.

Transformer couplings: As in the ideal configuration, the N_1 , N_2 coupling and the N_3 , N_4 coupling represent the first and second transformer couplings, respectively, where the first coupling is a step-up transformer and the second coupling is a step-down transformer.

Spherical capacitors: The same ideal configured capacitors, C , are represented on the diagram by a capacitor symbol wrapped in a circle, and are used as a transmitter-receiver system as before. The same detail work is conducted here to model the power transfer over the air gap between C_t and C_r .

Parasitic capacitance: This is the same as the ideal scenario. On the circuit diagram, the parasitic capacitors, C_p , represent the stray capacitance that the secondary coil on the transmitter and the primary coil on the receiver exhibit. This effect is negligible at low frequencies, but since the scope of the simulation extends to relatively high (~ 3 MHz) frequencies, parasitic capacitance must be accounted for.

Dual grounding: Similarly to the ideal case, there are two distinct “earth” grounds, v_{0_t} (for the transmitter circuit) and v_{0_r} (for the receiver circuit). The same qualities that plague the ideal case are present here, but the analysis relative to grounding becomes inherently more complicated in the non-ideal case.

Load on receiver: The same load that was present in the ideal case, Z_0 , is used here. Powering an LED in a non-ideal circuit like this may normally require in-depth discussion, but our main concern is whether the load is powered or not, so Z_0 is modelled as an Ohmic load for simplicity even in the non-ideal configuration.

4.2 Formulation

4.2.1 Circuit Analysis and Equivalence

For the non-ideal model, known quantities are absolutely crucial to simplicity for numerical solving. As in the ideal case, we may arbitrarily take v_{src} as sinusoidal with no initial phase offset:

$$v_{\text{src}}(t) = V_{\text{max}} \sin(\omega t).$$

We begin by attempting to find equivalent circuit segments for each independent “loop” of the circuit. To do this, we work with, and combine, impedances throughout the circuit on the first approach. This allows us to avoid the use of differential equations in a multi-coupled system. Under this paradigm, the individual component impedances are defined as below:

$$\begin{aligned} Z_{R1} &= R_1 & Z_{l1} &= j\omega L_{l1} & Z_{Ct} &= 1/j\omega C_t \\ Z_{R2} &= R_2 & Z_{l2} &= j\omega L_{l2} & Z_{Cp1} &= 1/j\omega C_{p1} \\ Z_{R3} &= R_3 & Z_{l3} &= j\omega L_{l3} & Z_{Cp2} &= 1/j\omega C_{p2} \\ Z_{R4} &= R_4 & Z_{l4} &= j\omega L_{l4} & Z_{Cr} &= 1/j\omega C_r \\ & & Z_{m1} &= j\omega L_{m1} & & \\ & & Z_{m2} &= j\omega L_{m2} & & \end{aligned}$$

We abbreviate this process by combining components that are in obvious series (see figure 4.1):

$$\begin{aligned} Z_1 &= Z_{R1} + Z_{l1} = R_1 + j\omega L_{l1}, \\ Z_2 &= Z_{R2} + Z_{l2} + Z_{Ct} = R_2 + j\omega L_{l2} + 1/j\omega C_t, \\ Z_3 &= Z_{R3} + Z_{l3} = R_3 + j\omega L_{l3}, \\ Z_4 &= Z_{R4} + Z_{l4} + Z_0 = R_4 + j\omega L_{l4} + Z_0. \end{aligned}$$

The modified circuit now takes on a simpler form, as seen in Figure 4.2.

(*Note:* Here, unconventional notation for the transformers is used, and is partially pared from notation utilized in [15] to describe a simpler version of an imperfect air core transformer. Mathematically, e_1 , e_2 , e_3 , and e_4 represent voltages across each side of the transformer couplings and hold the relationships such that $e_1 = L_{m1} \cdot di_{m1}/dt$,

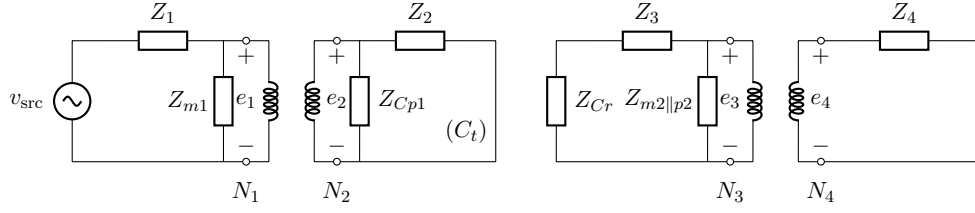


FIGURE 4.2: Experimental setup with series combined impedances

$e_2 = e_1 \cdot N_2/N_1$, $e_3 = L_{m2} \cdot di_{m2}/dt$, and $e_4 = e_3 \cdot N_4/N_3$. We may arbitrarily define $N_1/N_2 = a_1$ and $N_3/N_4 = a_2$ for ease of formulation and use. This notation is henceforth used extensively in our work.)

Now that in the second loop, Z_2 and Z_{Cp1} are in parallel, and in the third loop, Z_{m2} and Z_{Cp2} are in parallel (the second case being described on the diagram for brevity). Using this information, basic parallel impedance calculations can now be used to wrap the impedance “totals” together, simplifying the circuit even further. Below, each Z_{Tn} expression represents a combination:

$$\begin{aligned}
 Z_{T1} &= Z_1 = R_1 + j\omega L_{l1} \\
 Z_{T2} &= \left(\frac{1}{Z_2} + \frac{1}{Z_{Cp1}} \right)^{-1} = \left(\frac{1}{R_2 + j\omega L_{l2} + 1/j\omega C_t} + j\omega C_{p1} \right)^{-1} \\
 Z_{T3} &= \left(\frac{1}{Z_3} + \frac{1}{Z_{m2||p2}} \right)^{-1} = \left(\frac{1}{R_3 + j\omega L_{l3}} + \frac{1}{Z_{m2||p2}} \right)^{-1} \\
 Z_{T4} &= Z_4 = R_4 + j\omega L_{l4} + Z_0.
 \end{aligned}$$

Figure 4.3 illustrates how this system will look based on the combined impedances along leakage and resistance-of-medium. With this approach, we could begin more intensive analysis by applying KVL and KCL to the phasor forms of impedances of the symbolic, non-ideal quantities as well.

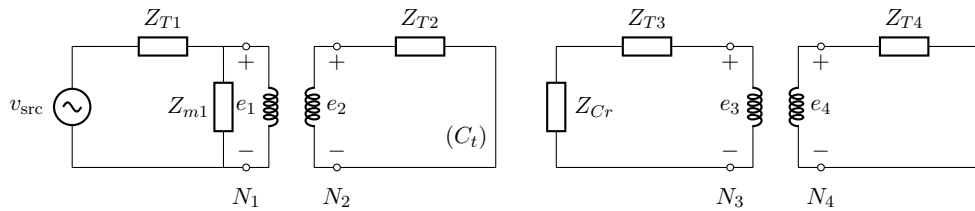


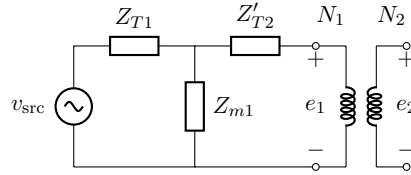
FIGURE 4.3: Experimental setup with combined impedances along medium resistance and medium leakage

However, linkage may be established by making use of properties of an ideal transformer:

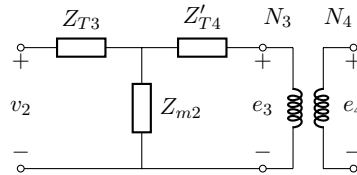
$$Z' = \left(\frac{N_p}{N_s}\right)^2 Z \iff Z = \left(\frac{N_s}{N_p}\right)^2 Z'.$$

This reflection of impedances is crucial, albeit routine for more involved transformer analysis. Despite accounting for losses in the transformer circuit, we are still able to assume ideal equations for the junction of the transformer junction; this is an exceptionally important part of analysis presented in [15] and similar earlier literature (see pp. 202-207 of [16] for an in-depth primary analysis of the “T” equivalent circuit). This also allows an equivalent conjunction of both circuits to be used, and significantly simplifies analysis by allowing an equivalent circuit to be used in place of a transformer by incorporating a_1 and a_2 factors.

For the lefthand circuit containing C_t across e_1 , the following diagram illustrates its equivalent by accounting for the transformer linkage from the primary side:



The same type of scaling can be used with the receiver circuit, with the main difference being the replacement of v_{src} with v_2 :



Each new simplified circuit contains a new referential quantity, Z'_{T2} and Z'_{T4} . Each of these new quantities makes use of the familiar turn ratios a_1 and a_2 , where $Z'_{T2} = (a_1)^2 Z_{T2}$ and $Z'_{T4} = (a_2)^2 Z_{T4}$, as described above. The simplified circuits take on elementary forms across e_1 and e_3 , so we may apply KVL and KCL once again. In the same manner as before, loop currents may be illustrated in order to aid in the mesh analysis of the circuit at the open terminals. An illustration of this is shown in Figure 4.4 for each circuit.

A tremendous benefit from this approach is that the transformer junction may now be treated as a short, provided that we account for the transformed voltage, current, and

impedance values using technical and mathematical gymnastics. Something else that must be accounted for as we approach the mesh analysis of the receiver and transmitter circuits, however, is that e_1 and e_3 are elevated by the transformer junctions to e_2 and e_4 , respectively, just as before. As a result, power and energy conservation must play a fundamental role in the logic behind this analysis, particularly for the discussion of transmission must be included. Thankfully, since the transformer junctions have been idealized by reflecting the loads Z_{T2} and Z_{T4} into Z'_{T2} and Z'_{T4} , much of this power conservation will *already* be accounted for, and separate analysis will be simple. For now, we turn our lens to the circuits at hand separately using well-known methods.

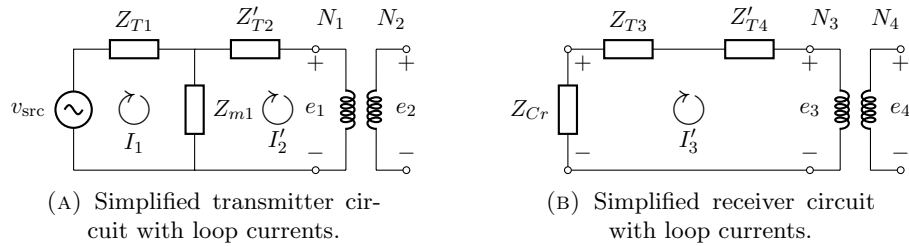


FIGURE 4.4: Setup for simplified analysis on both transmitter and receiver circuits.

Remember that the voltage for e_1 and e_3 may now be treated as mathematical shorts, since the load through e_2 and e_4 have been accounted for in Z'_{T2} and Z'_{T4} . To simplify this analysis further, we note that if the transformer junction behaves as a short, then Z'_{T2} is in parallel with Z_{m1} :

$$Z_{\parallel 1} = \left(\frac{1}{Z_{m1}} + \frac{1}{Z'_{T2}} \right)^{-1}.$$

For the receiver circuit, Z_{T3} is in series with Z'_{T4} :

$$Z_{T3+T4'} = Z_{T3} + Z'_{T4}.$$

Now, Z_{T1} is in series with $Z_{\parallel 1}$:

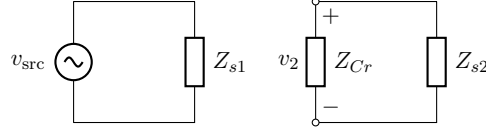
$$Z_{s1} = Z_{T1} + \left(\frac{1}{Z_{m1}} + \frac{1}{Z'_{T2}} \right)^{-1}.$$

Thus the two total impedances for the grouped circuits are

$$Z_{s1} = Z_{T1} + \left(\frac{1}{Z_{m1}} + \frac{1}{Z'_{T2}} \right)^{-1},$$

$$Z_{s2} = Z_{T3} + Z'_{T4}.$$

The following circuit diagrams illustrate this transformation:



Although this appears to be an oversimplification of the nonideal transformers' circuitry, one must remember that much of the conversion hinges on building the turn ratios, $a_1 = N_1/N_2$ and $a_2 = N_3/N_4$, into the circuit conversions mathematically. It is obvious from our simplified circuit that $v_{\text{src}} = I_t Z_{s1}$ and $v_2 = I_r Z_{s2}$ (where I_t and I_r are individual loop currents for the transmitter and receiver circuits, respectively), but the impedances may be written explicitly. Doing so yields multiple values in terms of inductances and turn ratios:

$$Z_{s1} = R_1 + j\omega L_{l1} + \left(\frac{1}{j\omega L_{m1}} + \frac{a_1^{-2}}{R_2 + j\omega L_{l2} + 1/j\omega C_t} + a_1^{-2} j\omega C_{p1} \right)^{-1},$$

$$Z_{s2} = a_2^2 (R_4 + j\omega L_{l4} + Z_0) + \left(\frac{1}{R_3 + j\omega L_{l3}} + \frac{1}{j\omega L_{m2}} + j\omega C_{p2} \right)^{-1}.$$

If we impose loop currents I_t and I_r for the transmitter and receiver circuits, we have that

$$v_{\text{src}} = I_t \left[R_1 + j\omega L_{l1} + \left(\frac{1}{j\omega L_{m1}} + \frac{a_1^{-2}}{R_2 + j\omega L_{l2} + 1/j\omega C_t} + a_1^{-2} j\omega C_{p1} \right)^{-1} \right], \quad (4.1)$$

$$v_2 = I_r \left[a_2^2 (R_4 + j\omega L_{l4} + Z_0) + \left(\frac{1}{R_3 + j\omega L_{l3}} + \frac{1}{j\omega L_{m2}} + j\omega C_{p2} \right)^{-1} \right]. \quad (4.2)$$

By using equation (4.1) to determine I_t , common methods for parallel and series circuits, including current division, may be used to determine the voltage across the transmitting capacitor, C_t , through use of its loading, Z_{Ct} , incorporated into Z'_{T2} . We are able to first create a system of equations using KVL and loop currents (see figures 4.2, 4.3, and 4.4):

$$\begin{bmatrix} Z_{T1} + Z_{m1} & -Z_{m1} \\ -Z_{m1} & a_1^2 Z_{p1||T2} + Z_{m1} \end{bmatrix} \begin{bmatrix} I_1 \\ I_2 \end{bmatrix} = \begin{bmatrix} v_{\text{src}} \\ 0 \end{bmatrix}.$$

A similar system may be found for the receiving circuit with input voltage v_2 , or more appropriately, v_{Cr} :

$$\begin{bmatrix} Z_{T3} + Z_{m2||p2} & -Z_{m2||p2} \\ -Z_{m2||p2} & a_2^2 Z_{T4} + Z_{m2||p2} \end{bmatrix} \begin{bmatrix} I_3 \\ I'_4 \end{bmatrix} = \begin{bmatrix} v_{Cr} \\ 0 \end{bmatrix}.$$

In the above systems, I_1 and I'_2 represent loop currents (with I'_2 travelling through the mirrored components) of the transmitter, while I_3 and I'_4 represent loop currents (with I'_4 travelling through the mirrored components) of the receiver. Solving both of these systems computationally, we obtain the results

$$\begin{bmatrix} I_1 \\ I'_2 \end{bmatrix} = \begin{bmatrix} -\frac{v_{src}(Z_{m1} + a_1^2 Z_{p1||T2})}{Z_{m1}^2 - (Z_{T1} + Z_{m1})(Z_{m1} + a_1^2 Z_{p1||T2})} \\ -\frac{v_{src} Z_{m1}}{Z_{m1}^2 - (Z_{T1} + Z_{m1})(Z_{m1} + a_1^2 Z_{p1||T2})} \end{bmatrix},$$

$$\begin{bmatrix} I_3 \\ I'_4 \end{bmatrix} = \begin{bmatrix} -\frac{v_{Cr}(a_2^2 Z_{T4} + Z_{m2||p2})}{Z_{m2||p2}^2 - (Z_{T3} + Z_{m2||p2})(Z_{m2||p2} + a_2^2 Z_{T4})} \\ -\frac{v_{Cr} Z_{m2||p2}}{Z_{m2||p2}^2 - (Z_{T3} + Z_{m2||p2})(Z_{m2||p2} + a_2^2 Z_{T4})} \end{bmatrix}.$$

Since I'_2 is the current that flows through Z'_{T2} , using simple current division from here allows us to find the current through Z_2 , defined here as I_a :

$$I_a = \frac{Z_{Cp1}}{Z_{Cp1} + Z_2} I'_2.$$

Similarly, we can find the current flowing through Z_0 , defined here as I_b , by simply appealing to the fact that Z'_{T4} is a series combination:

$$I_b = I'_4.$$

Note that since the impedance of the transmitting capacitor Z_{Ct} is a series element in Z_2 , taking $v_{Ct} = I_a Z_{Ct}$ will successfully find the voltage at the transmitting capacitor. Similarly, since Z_0 is a series element in Z'_{T4} , the same argument can be made using $e_4 = I_b Z_0$. Thus,

$$v_{Ct} = -\frac{Z_{Ct} Z_{Cp1}}{Z_{Cp1} + Z_2} \left[\frac{Z_{m1}}{Z_{m1}^2 - (Z_{T1} + Z_{m1})(Z_{m1} + a_1^2 Z_{p1||T2})} \right] v_{src}, \quad (4.3)$$

$$e_4 = - \left[\frac{Z_0 Z_{m2||p2}}{Z_{m2||p2}^2 - (Z_{T3} + Z_{m2||p2})(Z_{m2||p2} + a_2^2 Z_{T4})} \right] v_{Cr}. \quad (4.4)$$

4.2.2 Experimental Properties and Eccentric Physical Effects

Due to the less normative parameters of the experiment, multiple lesser-used electromagnetic properties exhibited in each part of the circuit must be examined. Notably, physical examination of these properties in [1] is somewhat lacking, but may still be accounted for by using the appropriate theory here. This presents an interesting secondary point to observe about our circuit model; namely, we examine these properties in detail here so that they may balance the simulation.

4.2.2.1 Equivalence Parameters

The primary coil, L_1 , of the transmitter has the same physical characteristics as the secondary coil of the receiver, L_4 , and the secondary coil of the transmitter, L_2 , has the same physical characteristics as the primary coil of the receiver, L_3 , such that

$$A_1 = A_4,$$

$$A_2 = A_3,$$

$$l_1 = l_4 = \pi \cdot d_1 \cdot n_1,$$

$$l_2 = l_3 = \pi \cdot d_2 \cdot n_2,$$

$$\rho_1 = \rho_2 = \rho_3 = \rho_4 = \rho_{Cu},$$

$$\mu_1 = \mu_2 = \mu_3 = \mu_4 = \mu_{Cu} = \kappa_{Cu} \mu_0.$$

Further, the following quantities are not only equivalent but measured, and given a match variable n for convenience:

$$N_1 = N_4 = n_1,$$

$$N_2 = N_3 = n_2.$$

This will prove to be immensely useful later.

4.2.2.2 Inductance and Geometry of Capacitors

Note here that the leakage inductances, L_l , and the magnetizing inductances, L_m , still require explicit definition, but there is something of a way around this using mutual

inductance. First, we make use of an esoteric property of leakage inductance used in [17], [18], and [19] that allows the primary coil's inductance, L_p , and the secondary coil's inductance, L_s , to be related to their mutual inductance factor, M . Leakage inductance on both sides of the transformer may then be accounted for using a coupling coefficient, k , defined similarly to a measure of efficiency, where we let $|M| = k\sqrt{L_p L_s}$ with $0 \leq k \leq 1$:

$$\begin{aligned} L_{lp} &= L_p - kL_p = L_p - \left(\frac{|M|}{\sqrt{L_p L_s}} \right) L_p, \\ L_{ls} &= L_s - kL_s = L_s - \left(\frac{|M|}{\sqrt{L_p L_s}} \right) L_s. \end{aligned}$$

Through basic algebraic manipulation, this becomes more approachable in terms of a , for which $a = N_p/N_s$:

$$\begin{aligned} L_{lp} &= L_p - \left(\frac{N_p}{N_s} \right) M = L_p - \left(\frac{N_p}{N_s} \right) k\sqrt{L_p L_s}, \\ L_{ls} &= L_s - \left(\frac{N_s}{N_p} \right) M = L_s - \left(\frac{N_s}{N_p} \right) k\sqrt{L_p L_s}. \end{aligned}$$

Calling on a similar method from [17], [18], and [19] allows the magnetizing inductance, L_m , of a transformer circuit to be related to the inductance of its primary coil, L_p , using a coupling factor, k , defined below in the standard way:

$$L_m = kL_p = \frac{|M|}{\sqrt{L_p L_s}} L_p = aM = \left(\frac{N_p}{N_s} \right) M = \left(\frac{N_p}{N_s} \right) k\sqrt{L_p L_s}.$$

Recall that k is a unitless coefficient, and $a = N_p/N_s = \sqrt{L_p/L_s}$; thus, the above relation works as expected without jeopardizing the integrity of the systems in question.

Several properties allow further simplification of this system to nearly pure algebra.

First, both transmitter and receiver capacitors have known a known radius r_C :

$$\left(\frac{d}{2} \right)_t = \left(\frac{d}{2} \right)_r = r_C.$$

This allows for many options of treatment for the conducting spheres that compose our capacitive system, which are detailed in a breakdown in Chapter 1.

Second, note that for a solenoidal inductor of turn count N , coil length l , and wire cross-sectional area A ,

$$L = \frac{N^2 \mu A}{l}.$$

However, for a general coil (such as a primary coil whose wire thickness is a sizeable fraction of its length), solenoidal assumptions may not necessarily be sufficient. An approximation (laid out in great detail in [20]) may be used such that

$$L \approx \frac{N^2 \mu d}{2} \left[\ln \left(\frac{4d}{r} \right) - 2 \right],$$

where d is the coil diameter and r is the wire radius (tolerably). This approximation is accurate to a sufficient degree - out to several decimal microhenries - and mitigates further terms of $O((l/r)^4)$. This accuracy more than suffices for our work, so exact forms of the approximation are not examined.

4.2.2.3 Resistance - Skin Effect, Proximity Effect, and Material Properties

For the thicker coils L_1 and L_4 , skin effect must be accounted for. As detailed in appendix A, the skin depth, δ , may be defined as

$$\delta = \sqrt{\frac{2\rho}{\omega\mu_{Cu}}}$$

for a good conductor such as copper. The attenuation effect this has on the thicker coils' resistances is notable compared to their width (8 awg, or 3.26 mm), and creates a dependency on the frequency ω . In particular, since the current density J can be measured with the skin effect as having, for some distance b from the surface of the conductor,

$$J = J_0 e^{-(1+j)b/\delta},$$

then the resistance may be defined somewhat intuitively by using energy conservation. (It should be noted that in the above formula, the imaginary component of the exponent is representative of phase lag only.) The cross sectional area of the wire in the coils, A_1 and A_4 , lends itself to the given current density J such that the current through the resisting wire, I , sets up simply as $I = JA$. Let $I_0 = J_0 A$ and R_0 be a geometric resistance

in the traditional way such that $R_0 = \rho l/A$. Then by energy (voltage) conservation,

$$I_0 R_0 = I_0 e^{-(1+j)^{b/\delta}} R \implies R = R_0 e^{(1+j)^{b/\delta}}.$$

So, the resistance of each (thicker) coil at depth b becomes a function of ω :

$$R_b = R_0 \exp \left[(1+j) \frac{b}{\sqrt{2\rho/\omega\mu}} \right]$$

or

$$R_b = R_0 \exp \left[(1+j)b \sqrt{\frac{\omega\mu}{2\rho}} \right].$$

This allows for a fixed ω to describe accurately the resistance of the interior of the thicker coils. When $b = 2\delta$, the resistance at this depth is 738% of the surface value, and at $b = 3\delta$, about 2,010% of the surface value. Consequently, a good approximation for a cross sectional area of our original resistor may in fact be a disk with thickness 3δ , centered by a hole. We account for this in the following way:

$$\begin{aligned} R_1 = R_4 &\approx \frac{\rho_{\text{Cu}} l_1}{\pi[r_1^2 - (3\delta - r_1)^2]} \\ &= \frac{\rho_{\text{Cu}} \pi \cdot d_1 \cdot 10}{\pi(r_1^2 - 9\delta^2 + 6\delta r_1 - r_1^2)} \\ &= \frac{\rho_{\text{Cu}} \cdot 10d_1}{3(2\delta r_1 - 3\delta^2)} \\ &= \frac{10d_1 \rho_{\text{Cu}}}{3(2\delta r_1 - 3\delta^2)}. \end{aligned}$$

The dependence of R_1 and R_4 on δ leads to a dependence on ω :

$$R_1 = R_4 \approx \frac{10d_1 \rho_{\text{Cu}}}{3 \left(2r_1 \sqrt{\frac{2\rho_{\text{Cu}}}{\omega\mu_{\text{Cu}}}} - \frac{6\rho_{\text{Cu}}}{\omega\mu_{\text{Cu}}} \right)}. \quad (4.5)$$

Each of these pieces of information helps to frame the laboratory setup around two things: one, the voltage (and current) being induced across (and through) C_t , and two, the voltage being measured at v_2 (and in turn across C_r). Thanks to nearly all of the information about each coil and capacitor being known, this process becomes much simpler, despite the somewhat nasty setup above.

4.2.3 Capacitor Field Interactions

For the non-ideal model, we make use of the same field approximations as what was used in §3.2.3. This means taking another elementary potential difference along a single-lined path by modelling the capacitor field interactions as the interactions of two separate capacitors with a transmitting electric field, \vec{E} , between them. (Note that this was already assumed in earlier model constructions in this chapter for the explicit construction of the transmitter and receiver circuits, even in the non-ideal case.)

Besides the more complicated impedance coefficient, the approximation is largely the same, and makes use of the same variables (again, our precise electric potential is represented by ϕ):

$$\vec{E} = -\nabla\phi \longrightarrow E = -\frac{\partial\phi}{\partial x}.$$

First, finding the capacitance is similar to the ideal case, where both capacitors have a radius r_C :

$$C_t = C_r = 4\pi\epsilon r_C.$$

Similarly, we appeal to the fact that $Q = VC$ for any capacitor. As such, for the transmitting capacitor,

$$\begin{aligned} Q_{Ct} &= v_{Ct} \cdot C_t = -\frac{Z_{Ct}Z_{Cp1}}{Z_{Cp1} + Z_2} \left[\frac{Z_{m1}}{Z_{m1}^2 - (Z_{T1} + Z_{m1})(Z_{m1} + a_1^2 Z_{p1||T2})} \right] v_{src} \cdot 4\pi\epsilon_0 r_C \\ &= z v_{src} \cdot 4\pi\epsilon_0 r_C, \end{aligned}$$

where z is an impedance coefficient as a function of ω implicitly. Now, using the electric field of a sphere of charge, we substitute for Q :

$$\vec{E} = \frac{z v_{src} r_C}{r^2} \hat{r}.$$

Besides the more complicated impedance coefficient, the \vec{E} field approximation is largely the same as that in §3.2.3, and makes use of the same variables (again, our precise electric potential is represented by ϕ , and the path is assumed monodirectional):

$$\vec{E} = -\nabla\phi \longrightarrow E = -\frac{\partial\phi}{\partial x} \approx -\frac{\Delta V}{\Delta x},$$

$$\Delta V = -E\Delta x = -E\Delta r.$$

Substituting for the change in voltage ΔV , the path Δr and E , we get

$$v_{Cr} = v_{Ct} - \frac{zv_{src}r_C}{r_r^2}(r_r - 0) = v_{Ct} - \frac{zv_{src}r_C}{r_r}.$$

(Note again that $r_t = 0$ as reference.) Now by substituting for v_{Ct} explicitly,

$$v_{Cr} = -v_{src} \frac{Z_{Ct}Z_{Cp1}}{Z_{Cp1} + Z_2} \left[\frac{Z_{m1}}{Z_{m1}^2 - (Z_{T1} + Z_{m1})(Z_{m1} + a_1^2 Z_{p1||T2})} \right] \left[1 - \frac{r_C}{r_r} \right]. \quad (4.6)$$

The complexity of these calculations is expounded in the following section (§4.3).

4.3 End Computation

4.3.1 Symbolic Computational Forms

By substituting equation (4.6) into (4.4), a complicated unifying equation is created. For convenience, we describe this in compressed notation as a phasor function of ω :

$$e_4(\omega) = z_t(\omega)z_r(\omega)V_{\max} \left(1 - \frac{r_C}{r_r} \right), \quad (4.7)$$

where z_t and z_r are defined as

$$z_t(\omega) = -\frac{Z_{Ct}Z_{Cp1}}{Z_{Cp1} + Z_2} \left[\frac{Z_{m1}}{Z_{m1}^2 - (Z_{T1} + Z_{m1})(Z_{m1} + a_1^2 Z_{p1||T2})} \right],$$

$$z_r(\omega) = -\left[\frac{Z_0 Z_{m2||p2}}{Z_{m2||p2}^2 - (Z_{T3} + Z_{m2||p2})(Z_{m2||p2} + a_2^2 Z_{T4})} \right].$$

with the following composite impedances:

$$Z_{T1} = Z_1 = R_1 + j\omega L_{l1},$$

$$Z_{T2} = \left(\frac{1}{Z_2} + \frac{1}{Z_{Cp1}} \right)^{-1} = \left(\frac{1}{R_2 + j\omega L_{l2} + 1/j\omega C_t} + j\omega C_{p1} \right)^{-1},$$

$$Z_{T3} = \left(\frac{1}{Z_3} + \frac{1}{Z_{m2||p2}} \right)^{-1} = \left(\frac{1}{R_3 + j\omega L_{l3}} + \frac{1}{Z_{m2||p2}} \right)^{-1},$$

$$Z_{T4} = Z_4 = R_4 + j\omega L_{l4} + Z_0,$$

$$Z_{Cp1} = -j/\omega C_{p1},$$

$$Z_{Cp2} = -j/\omega C_{p2},$$

$$\begin{aligned} Z_{Ct} &= -j/\omega C_t, \\ Z_{m1} &= j\omega L_{m1}, \\ Z_{m2} &= j\omega L_{m2}. \end{aligned}$$

Note that the phasor representation of v_{src} is simply V_{max} . This highlights an interesting comparison: despite the initial complexity, equation (4.9) bears a striking resemblance to the ideal case of equation (3.3) in §3.3. However, the main, most difficult difference is that a substantial portion of the non-ideal case is controlled by frequency outside of the AC voltage input. It should also be noted that R_1 and R_4 are both skin effect functions of ω (see §4.2.2.3). Both $z_t(\omega)$ and $z_r(\omega)$ would be extensively difficult to manually simplify to a rectangular form of a complex number; however, numerical computation may now take place while working with the knowledge that both R_1 and R_4 are functions of ω . Despite this, the output voltage e_4 can still be described as the composite of these functions, and therefore a function of the frequency ω itself.

4.3.2 Component Numerical Information

Work must now be done to evaluate each of the constants present in equation (4.11). Some of these constants are easier than others, while some require conditions laid out in §4.2.

Resistances R_1 and R_4 are found by accounting for skin-effect driven geometry and show frequency dependence, as described in §4.2, whereas resistances R_2 and R_3 are found using the rudimentary resistance formula and yield a constant:

$$\begin{aligned} R_1 = R_4 &= \frac{3.42 \Omega}{10^6 \left(\sqrt{\frac{0.0267}{\omega}} - \frac{0.0802}{\omega} \right)}, \\ R_2 = R_3 &= 51.6 \Omega. \end{aligned}$$

For the inductances of each coil, constants are found as well:

$$\begin{aligned} L_1 = L_4 &= 5.22 \times 10^{-5} \text{ H or } 52.2 \mu\text{H}, \\ L_2 = L_3 &= 0.168 \text{ H or } 1.68 \times 10^5 \mu\text{H}. \end{aligned}$$

From these, the magnetizing and leakage values, L_m and L_l , are found for the transmitter and receiver circuits. These non-ideal quantities have a dependence on the coupling

coefficient k :

$$L_{l1} = L_{l4} = 52.2 - 29.6k \text{ } \mu\text{H},$$

$$L_{l2} = L_{l3} = (1.68 - 2.96k) \times 10^5 \text{ } \mu\text{H},$$

$$L_{m1} = 29.6k \text{ } \mu\text{H},$$

$$L_{m2} = 2.96k \times 10^5 \text{ } \mu\text{H}.$$

Note that both L_{l2} and L_{l3} will only exhibit non-negative inductance when $k \leq 0.568$. We therefore consider this value of coupling as a critical point, as values greater than 0.568 theoretically create negative leakage inductance.

We evaluate the capacitors differently depending on their role in the circuit. For the spherical capacitors C_t and C_r , we have that

$$C_t = C_r = 6.673 \times 10^{-12} \text{ F or } 6.673 \text{ pF}.$$

For the parasitic capacitance C_{p1} and C_{p2} , we make use of Medhurst's formula (see Appendix A and Appendix C) with a cubic interpolated H value for $l/D = 5.1$ for C_{p1} and C_{p2} , similar to chapter 3:

$$C_{p1} = C_{p2} = 4.274 \text{ pF}.$$

Accounting for each of the functions of k and the separate functions of ω puts a high degree of complexity on solving for this model. One can see certain singularities that arise in the denominator of the expression, but simulation is still essential even for numerical results.

Chapter 5

Simulation Results

Based on information from the ideal and non-ideal models, throughput voltage curves were modelled fairly successfully in both cases in regard to data compared. Strange discrepancies did manifest, some of which may be due to the simplicity of the assumed geometry regarding the electric field and the capacitor interactions.

5.1 Ideal Model

Results for the ideal model behaved almost exactly like a diminishing voltage throughput, with very little evidence that resonance occurs on its own. In Figure 5.1, the red series is the voltage across the load in the lab setup. As can be seen in this comparison against Figure 5.2, the ideal simulation as constructed was not useful for locating resonant frequencies. It should be noted that the general trend of max magnitude of the voltage across the load, however, was extremely close asymptotically. The simulation behaves strangely around low frequencies, but this is to be expected – this project focused exclusively on higher frequency ranges to model.

5.2 Non-ideal Model

(See pages 32-33 for figures.)

For the non-ideal model (Figures 5.3, 5.4, and 5.5), we simulated several different coupling coefficients between each set of coils on the transmitter and receiver, and achieved good results. It is immediately clear that the non-ideal model is a much better fit, and even serves to locate a resonant frequency between 1.5 and 1.75 MHz that shows up

in the data collected as well. Strangely, this resonance frequency happens only at extremely low coupling between the primary and secondary coils on each side ($k = 0.1$). Other resonances show up near the low frequency range, and spike to magnitudes well beyond feasible for the circuit, but this is mathematically and computationally expected, as this indicates computational singularity around these points as desired. The largest match that we see is around the 500 kHz region, in which the spikes simulated by the students at UCO using COMSOL Multiphysics match up extraordinarily well with the spikes evaluated in our model. A particularly critical transfer happens when $k = 0.568$, and this shows here as well. The resonance about this region is extremely high even for a computationally desired result, and when modelling with lower ticks between domain points, the curve for $k = 0.568$ dropped off substantially. This seems to indicate an extremely narrow band – between 250 kHz and 750 kHz – that seems to result in spiked power transfer via resonance. This is especially true when compared with the modelled (blue) and actual (red) curves of the UCO design group. Another strange phenomenon that seems to occur is the lining up of phase drops and peaks with resonant frequencies, particularly along a curve of extremely high phase values that travels back to the extremes (from about 2MHz at $k = 0.2$ to 4 MHz at $2 < k < 4$). There is a pattern to this phase distribution, but it lies beyond the scope of this work.

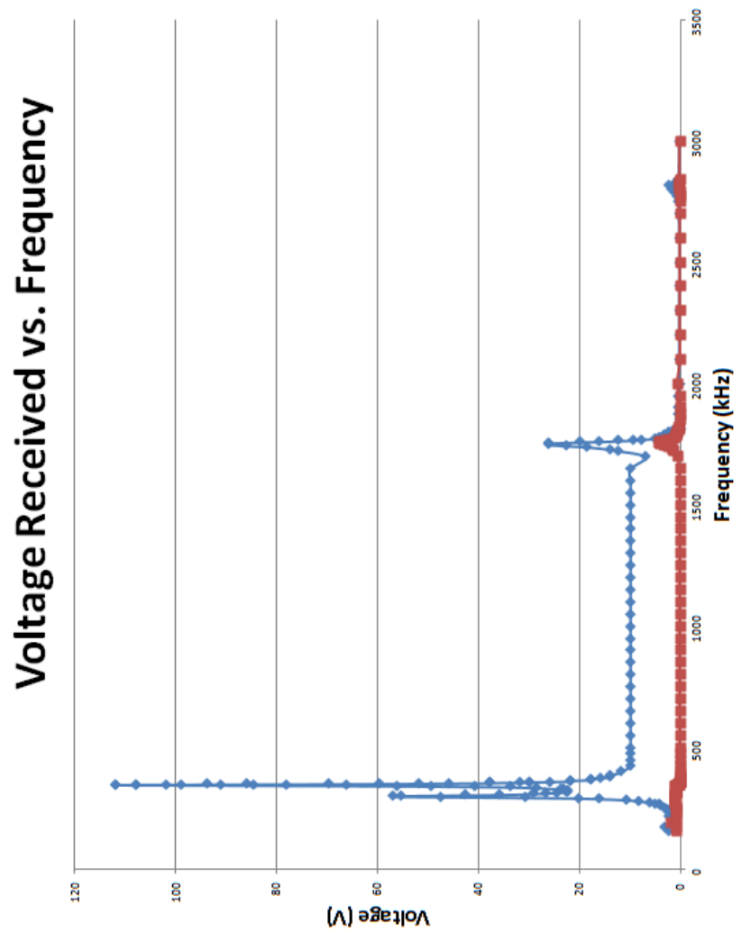


FIGURE 5.1: Lab results of physical study

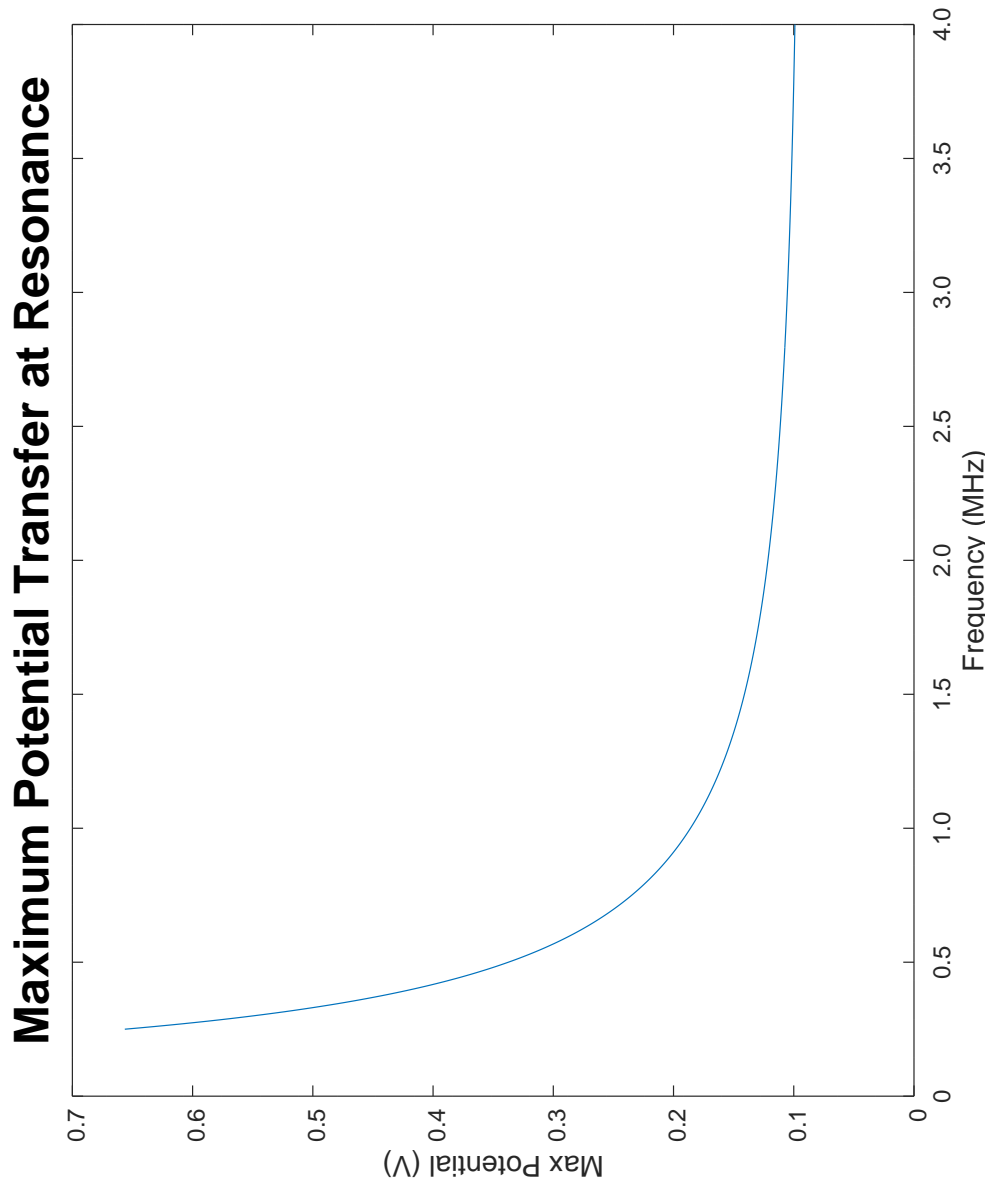
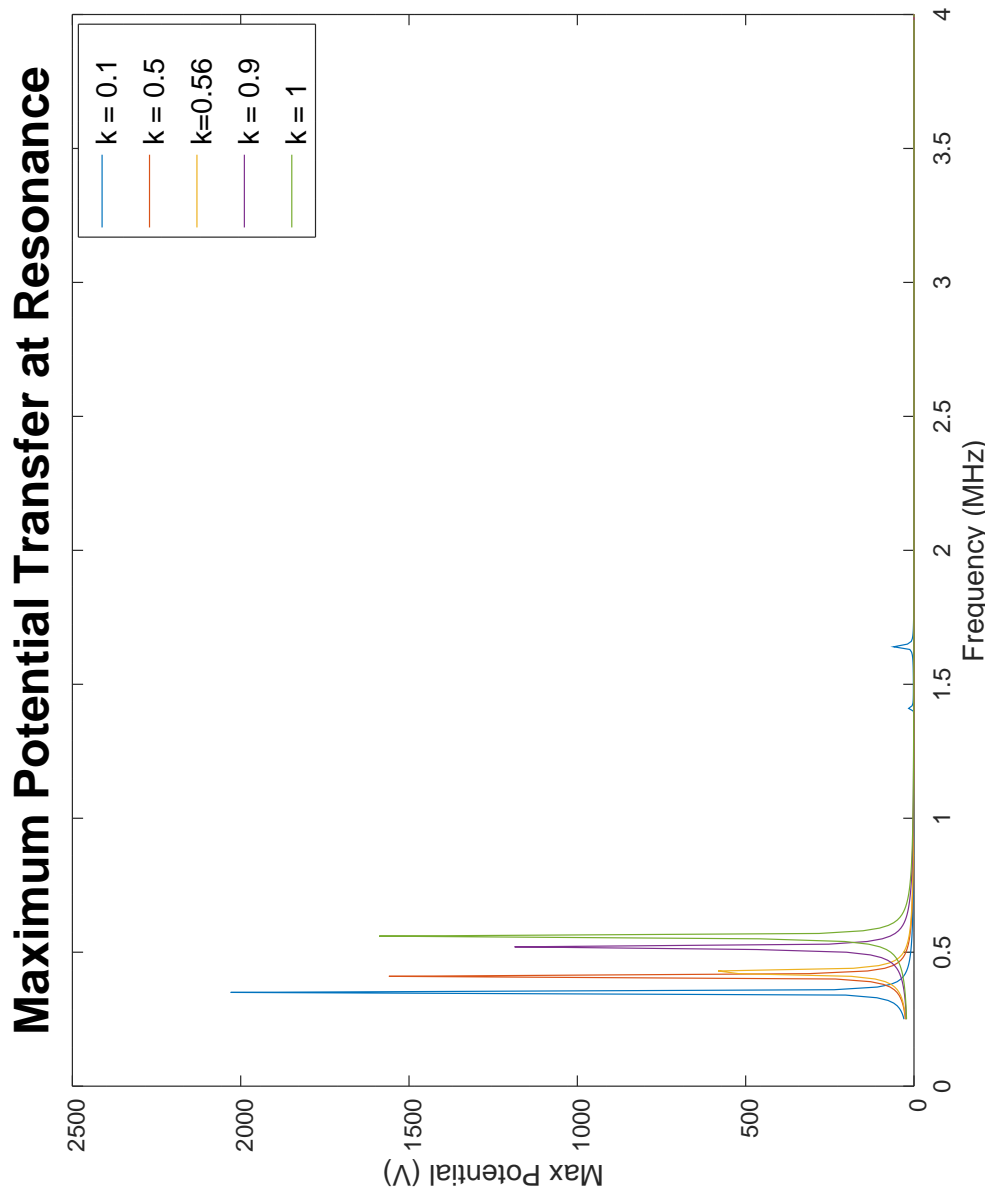
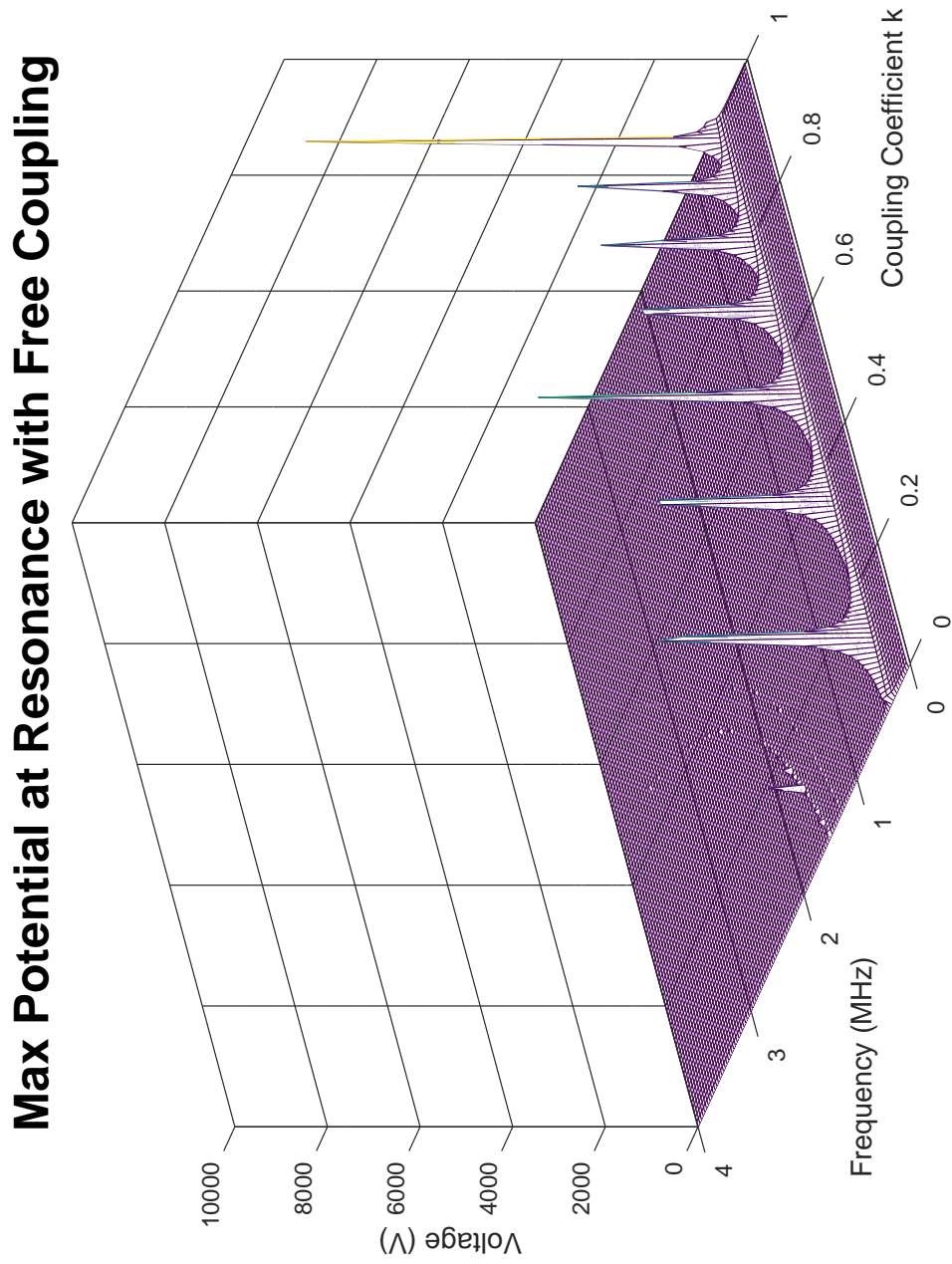
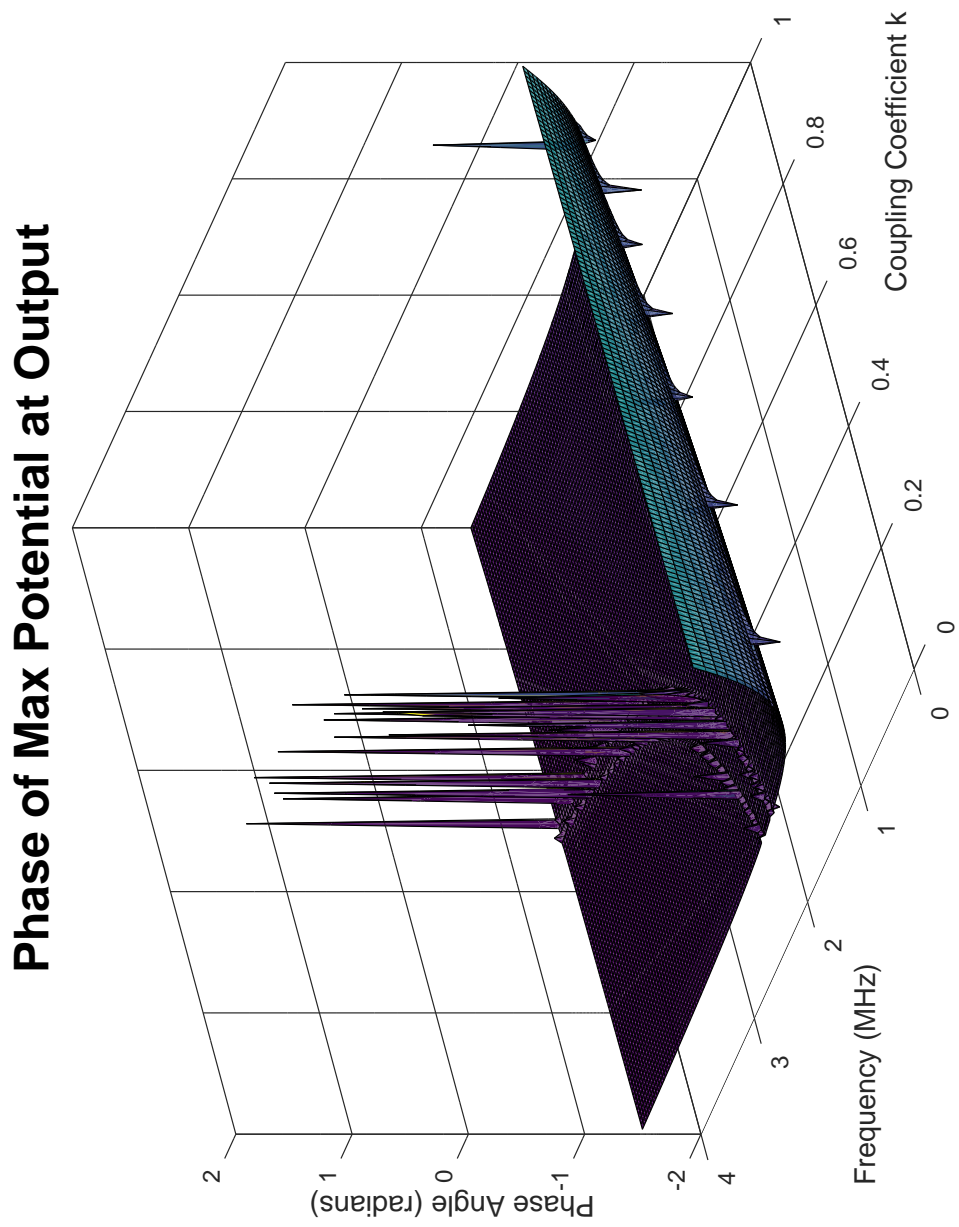


FIGURE 5.2: Ideal simulation results

FIGURE 5.3: Non-ideal simulation results at fixed k values

FIGURE 5.4: Non-ideal simulation results with free coupling k

FIGURE 5.5: Phase as a function of free coupling k and frequency ω

Chapter 6

Conclusions

As may have been expected, the ideal model utilizing first approximation of spherical capacitor interaction did not perform well. No clear discernible resonant frequencies were found, and the model behaved for the most part as though no resonance, except near the origin, could take place. Even this was questionable, as our model was only designed for high frequency purposes. However, the magnitude of the ideal model was, for the most part, on par with the lab results we compared against. Still, this certainly indicates a need for deeper consideration, even in the ideal case, than just parasitic capacitance.

On the other hand, the non-ideal model performed excellently. Calculated results and physical results from the UCO research group matched up very well with the non-ideal simulated results, and even found substantial overlap at a resonance between 1.5 and 1.75 MHz. However, results of our simulations seem to indicate that exterior factors are at play as well: for reasons beyond the scope of investigation of this project, it seems that the more efficient the coupling between the coils on the transmitter and receiver, the less likely a resonant frequency is to arise. This could be, in part, due to the heavy load placed on the system by considerations of magnetizing and leakage inductance, but the most consistent pattern was that of the resonant spikes between 250 and 750 kHz. No matter what the coupling coefficient was, there was always a resonant spike in this region. A pattern of phase drops emerged based on frequency and coupling coefficient as well. Perhaps most surprisingly, though, was the fact that modelling the transmitting and receiving spheres as two separate capacitors separated by a linear distance was nearly sufficient for simulating real world data. This admittedly defied expectations,

and reaffirmed that basic approximations in this regard work well for limited capacity applications, and even more so demonstrated feasibility that is essential to the survival of this approach to WPT.

Because of the unexpected behavior of our non-ideal simulation, opportunity for extensibility is ripe. For example, the coupling coefficient k was controlled to be the same value on either side of the non-ideal circuit. In reality, this could vary, perhaps even over time as per saturation by the magnetic flux, independently of each side. Another investigation could be done into one of the other methods of dealing with the capacitance of the spheres, such as treating them as a single capacitor of two adjacent spheres across an air gap as laid out in Chapter 1. This could mitigate some of the unknown offset that we see with the treatment of a linear electric field between C_t and C_r , and account for more electric flux at the receiving sphere. A magnetic circuit differential equation version of this system should be investigated further, especially one that may account for saturation and fluctuation in magnetic reluctance.

While the ideal model was uneventful in its results, the non-ideal model was a much better (if strange) fit, and illustrated an important, and somewhat unaccounted for, relationship between the coupling coefficient k , frequency ω , and resonant voltage.

Appendix A

Formulas

See Appendix E for more information regarding empirical formulas used in this section.

1. Maxwell's Equations (differential form):

$$\begin{aligned}\nabla \cdot \vec{E} &= \frac{\rho}{\epsilon_0}, \\ \nabla \times \vec{E} &= -\frac{\partial \vec{B}}{\partial t}, \\ \nabla \cdot \vec{B} &= 0, \\ \nabla \times \vec{B} &= \mu_0 \vec{J} + \mu_0 \epsilon_0 \frac{\partial \vec{E}}{\partial t},\end{aligned}$$

where ρ is the charge density with respect to a certain volume or other geometry, and \vec{J} is the current density.

2. Maxwell's Equations (integro-differential form):

$$\begin{aligned}\oiint_{\partial V} \vec{E} \cdot d\vec{A} &= \frac{Q_{\text{enc}}}{\epsilon_0}, \\ \oiint_{\partial V} \vec{B} \cdot d\vec{A} &= 0, \\ \oint_{\partial S} \vec{E} \cdot d\vec{L} &= -\iint_S \frac{\partial \vec{B}}{\partial t} \cdot d\vec{A}, \\ \oint_{\partial S} \vec{B} \cdot d\vec{L} &= \mu_0 I_{\text{enc}} + \mu_0 \epsilon_0 \iint_S \frac{\partial \vec{E}}{\partial t} \cdot d\vec{A},\end{aligned}$$

where an isolated ∂X indicates the boundary that encloses a given surface (or volume) X . (The variables S and V are such a surface and volume, respectively.)

3. Faraday's Law:

$$\mathcal{E} = -N \frac{d\Phi_B}{dt},$$

where N is the number of turns in a given coil, and for magnetic field \vec{B} and normal area vector \vec{A} , the magnetic flux Φ_B is as

$$\Phi_B = \iint_S \vec{B} \cdot d\vec{A} = BA \cos \theta = B_{\perp} A.$$

4. Capacitance:

$$Q = VC,$$

$$i(t) = C \frac{dv}{dt}.$$

Note that this is the “classic” formula regarding the differential relationship between current, $i(t)$, and voltage, $v(t)$, as functions of time with a constant scale factor capacitance, C . This is also applicable in a limited number of cases to self-capacitance of a surface, plate, or other geometry (such as a conducting, non-hollow sphere); however, the context of this experiment and model is only centered on uses that this differential relationship may have for typical capacitance. In all reality, the demands for this formula are not extraordinary in this work.

5. Capacitance of two concentric conductive hollow spheres:

$$C = \frac{4\pi\epsilon_0}{\frac{1}{r_1} - \frac{1}{r_2}} = \frac{4\pi\epsilon_0 r_1 r_2}{r_2 - r_1},$$

where r_1 and r_2 are the radii of the interior and the outer sphere, respectively. As these spheres are separated only by air, the permittivity and permeability may be treated as those used for free space (ϵ_0 and μ_0) for the region between the interior facing surfaces of the spheres. Note that this capacitance could be directly improved by modifying the separation medium in the interior space separating the two spheres, such that $\epsilon = \epsilon_r \epsilon_0$ with a relative permittivity of $\epsilon_r > 1$.

6. Ohm's Law:

$$\vec{J} = \sigma \vec{E},$$

or

$$\vec{E} = \rho \vec{J},$$

where \vec{E} is the electric field motivating a current density \vec{J} travelling through a component or material of the given conductivity σ or resistivity ρ . For a certain resistor or load with resistance R , an easier form is

$$V = IR,$$

where V is the voltage across the component and I is the current flowing through it. For an AC circuit,

$$V = IZ,$$

where Z is the general impedance of a component, while V and I still represent voltage and current, respectively. These latter two forms are used most often through this work.

7. Voltage through an inductor along a circuit:

$$v(t) = L \frac{di}{dt}.$$

In the context of inductance through the coils used in experimentation, one must apply caution in using a simple relationship such as this for the correct context. Here, the voltage, $v(t)$, is related to the current, $i(t)$, through a scale factor of inductance, L , that is used in the context of self-inductance and energy storage through the utilization of a magnetic field. The use of mutual inductance may be important, but the typical use of self-inductance L in this work will be through resonant frequency calculations, among other esoteric applications.

8. Self-inductance of a solenoid:

For a solenoid, or coil inductor, its self inductance L is give by

$$L = \frac{N^2 \mu A}{l},$$

where N is the number of turns of the coil, μ is the coil material's permeability (such that $\mu = \mu_r \mu_0$, where μ_r is the relative permeability), A is the coiled wire's cross-sectional area, and l is the coiled wire's length.

9. Self-capacitance of a helical inductor or solenoid (empirical) [21] [22]:

$$C_s = H \cdot d,$$

where d is the diameter of the coil (in centimeters), and H is a proportionality constant correlated to l/d (length to diameter), and is determined empirically based on tabulated data (see Appendix E).

10. Wheeler's formula for inductance through an inverted cone coil (see [23] and [24] for more discussion on the helical component of this equation):

$$\begin{aligned} L_1 &= \frac{(Nr_{\text{ave}})^2}{9r + 10h}, \\ L_2 &= \frac{(Nr_{\text{ave}})^2}{8r + 11w}, \\ L &= \sqrt{(L_1)^2 \sin^2 \alpha + (L_2)^2 \cos^2 \alpha}, \end{aligned}$$

where N is the number of turns in the coil, L_1 is the helix factor of inductance, L_2 is the spiral factor of inductance, L is the total inductance, w is the effective width of the coil (in inches), h is the height of the coil (in inches), r_{ave} is the average radius of the coil (in inches), and α is the rise angle in degrees. Note that all inductances in this formula are measured in microhenries (μH), and that the conversion between inches and centimeters is $1 \text{ in} = 2.54 \text{ cm}$. In this formula, there exists a nondescript conversion factor (implicitly) between inches and microhenries.

11. Electromagnetic waves (general form):

$$\vec{E} = \vec{E}_0 \cos(\pm \omega t \pm \beta x),$$

$$\vec{B} = \frac{\vec{E}}{c'},$$

where for wave number β , wave velocity c' , and frequency ω ,

$$c' = \frac{\omega}{\beta}.$$

12. Electromagnetic waves in lossy dielectric media (see [25]):

For a lossy medium with a given permittivity ϵ , resistivity ρ , and conductivity σ ,

$$\begin{aligned}\vec{E} &= \vec{E}_0 e^{-\alpha x} \cos(\omega t \pm \beta x), \\ \vec{H} &= \frac{\vec{E}_0}{|\eta|} e^{-\alpha x} \cos(\omega t \pm \beta x - \theta_\eta),\end{aligned}$$

where, for attenuation α , wave number β , intrinsic impedance η , and loss angle θ ,

$$\begin{aligned}\alpha &= \omega \sqrt{\frac{\mu\epsilon}{2} \left[\sqrt{1 + \left[\frac{\sigma}{\omega\epsilon} \right]^2} - 1 \right]}, \\ \beta &= \omega \sqrt{\frac{\mu\epsilon}{2} \left[\sqrt{1 + \left[\frac{\sigma}{\omega\epsilon} \right]^2} + 1 \right]}, \\ |\eta| &= \sqrt{\frac{\mu/\epsilon}{\sqrt{1 + \left[\frac{\sigma}{\omega\epsilon} \right]^2}}}, \\ \tan 2\theta_\eta &= \tan \theta = \frac{\sigma}{\omega\epsilon},\end{aligned}$$

where $0 \leq \theta_\eta \leq \pi/4$.

13. Skin depth of an electromagnetic wave propagating in a conductor:

For a conductive medium of a given permittivity ϵ , resistivity ρ , and conductivity σ , the depth of penetration that an electromagnetic wave can travel before being attenuated by a factor of e^{-1} (or about 37%) is described by δ :

$$\begin{aligned}\delta &= \sqrt{\frac{2\rho}{\omega\mu}} \sqrt{\sqrt{1 + (\rho\omega\epsilon)^2} + \rho\omega\epsilon}, \\ \delta &= \frac{1}{\alpha} \text{ for sufficiently large } \sigma/\text{sufficiently small } \rho,\end{aligned}$$

where $\alpha = \beta = \sqrt{\pi f \mu \sigma}$. For most materials that are not ferromagnetic, permeability is near that of free space; that is, $\mu \approx \mu_0$. As before, $\vec{E} = \vec{E}_0 e^{-\alpha x} \cos(\omega t \pm \beta x)$.

Appendix B

Code

Octave was utilized to construct numerical solutions and a simulation of both the ideal and non-ideal scenarios, with care taken to preserve MATLAB syntax for backwards compatibility. As in our discussion, each portion of our simulation is divided into both ideal and non-ideal scripted `.m` files.

B.1 Ideal Simulation

```
% Auxiliary constant declarations.
C_tr = 6.673e-12;
C_p12 = 4.274e-12;
n1 = 10;
n2 = 1000;
Vmax = 15;
rC = 0.06;
rr = 1;
rt = 0;

% Z_0 modelled as a constant resistance of 13 ohm based
% around common LED assumptions.
Z_0 = 13;
vcr = (n2/n1) * Vmax * (1 - rC * (rr - rt)/(rr^2));

% vout function declaration, and evaluation of max voltage
% through. Variables "coef" and "denomcoef" are coefficients
% outside of the main expression and by omega on the
% denominator, respectively.
```

```

coef = vcr*C_p12/(1000/10)^2 /C_tr;
denomcoef = (1000/10)^2 * Z_0 * C_p12;
vout = @(w) coef .* (1.-j.*1./(denomcoef.*w));
realvout = @(w) real(vout(w));
imagvout = @(w) imag(vout(w));
voutmax = @(w) sqrt((real(vout(w))).^2 + (imag(vout(w))).^2);

%Input values for function voltage function.
x = [250e3:5e3:4000e3];

% Output values of maximum transfer.
ymax = voutmax(x);

h = figure(1);
linewidth = 3;
plot(x,ymax);

hx = xlabel('Frequency (MHz)');
hy = ylabel('Max Potential (V)');
ht = title('Maximum Potential Transfer at Resonance');
set(h,"papersize",[10,10]);
set(hx,"fontsize",12);
set(hy,"fontsize",12);
set(ht,"fontsize",20);
set(gca,'XTick',[0:500e3:4000e3]);
set(gca,"XTickLabel",'0','0.5','1.0','1.5','2.0','2.5','3.0','3.5','4.0');

```

B.2 Non-ideal Simulation

```

% Non-ideal experimental scenario. Here, a convention is used
% such that '14' symbolizes a quantity both applicable to
% coils 1 and 4, '23' symbolizes a quantity applicable to
% both coils 2 and 3, and 'tr' symbolizes a quantity applicable
% to both the transmitter and receiver.

% Auxiliary constant declarations.
R_23 = 51.6;
L_14 = 5.22e-5;

```

```

L_23 = 0.168;
C_tr = 6.673e-12;
C_p12 = 4.474e-12;
a_1 = 0.01;
a_2 = 100;
Vmax = 15;
rC = 0.06;
rr = 1;
rt = 0;

% Z_0 modelled as a constant resistance of 13 ohm used
% for simplicity (common LED saturation slope resistance).
Z_0 = 13;

% Passable function declarations. Here, 'w' represents the
% frequency omega, and 'k' is the coupling coefficient as
% expected. Note that these functions quickly become
% variable-dependent on both k and w.

% Auxiliary functions.
R_14 = @(w) 3.42 ./ ((sqrt(0.0267./w)-0.0802./w) .* 10^6);
Lleak14 = @(k) (52.2 .- 29.6.*k).*10^(-6);
Lleak23 = @(k) (1.68 .- 2.96.*k)*0.1;
Lmag1 = @(k) 29.6.*k;
Lmag2 = @(k) (2.96.*k).*0.1;

% Impedance functions for zt and zr.
ZCp = @(w) 1./(j.*w.*C_p12);
ZCt = @(w) 1./(j.*w.*C_tr);
Zm1 = @(k,w) j.*w.*Lmag1(k);
Zm2 = @(k,w) j.*w.*Lmag2(k);
Zm2p2 = @(k,w) (1./(Zm2(k,w)) .+ 1./(ZCp(w))).^(-1);
ZT1 = @(k,w) R_14(w) .+ j.*w.*Lleak14(k);
ZT2 = @(k,w) (1./(R_23 .+ j.*w.*Lleak23(k) .+ 1./(j.*w.*C_tr))
 .+ j.*w.*C_p12).^(-1);
Zp1T2 = @(k,w) (1./(ZCp(w)) .+ 1./(ZT2(k,w))).^(-1);
ZT3 = @(k,w) (1./(R_23.+j.*w.*Lleak23(k)) .+ 1./(Zm2p2(k,w)));
ZT4 = @(k,w) R_14(w) .+ j.*w.*Lleak14(k) .+ Z_0;

```

```

Z2 = @(k,w) R_23 .* j.*w.*Lleak23(k) .* 1./(j.*w.*C_tr);

% Numerator and denominator variables for zt and zr.
numzt = @(k,w) -1 .*ZCt(w).*ZCp(w).*Zm1(k,w);
numzr = @(k,w) -1 .*Z_0.*Zm2p2(k,w);
denzt = @(k,w) (ZCp(w).+ Z2(k,w)) .* ((Zm1(k,w)).^2
    .- (ZT1(k,w).+Zm1(k,w)).*(Zm1(k,w) .+ a_1.^2 .* Zp1T2(k,w)));
denzr = @(k,w) Zm2p2(k,w).^2 - (ZT3(k,w) .+ Zm2p2(k,w))
    .*(Zm2p2(k,w) .+ a_2.^2 .* ZT4(k,w));

% Declaration of zr and zt.
zt = @(k,w) numzt(k,w) ./ denzt(k,w);
zr = @(k,w) numzr(k,w) ./ denzr(k,w);

% Evaluation of e4, rectangular phasor form.
e4 = @(k,w) zt(k,w).*zr(k,w).*Vmax.*(1.-(rC.*(rr.-rt))./(rr.^2));

% Input for inverse tangent for e4.
tanres = @(k,w) imag(e4(k,w)) ./ real(e4(k,w));
phase = @(k,w) atan(tanres(k,w));

% Amplitude of sinusoidal form of e4.
e4max = @(k,w) abs(e4(k,w));

% e4max calculations at coupled values of raising efficiency:
% k = 0.1, k = 0.1, k = 0.5, k = 0.9, and k = 1.
e4maxlc = @(w) e4max(0.1,w);
e4maxmc = @(w) e4max(0.5,w);
e4maxcc = @(w) e4max(0.568,w);
e4maxhc = @(w) e4max(0.9,w);
e4maxpc = @(w) e4max(1,w);

% Input values for frequency.

```

```
x = [250e3:10e3:4000e3];

% Output values of maximum transfer at each coupling.
ymaxlc = e4maxlc(x);
ymaxmc = e4maxmc(x);
ymaxcc = e4maxcc(x);
ymaxhc = e4maxhc(x);
ymaxpc = e4maxpc(x);

% Figure 1: Max potential transfer.
h = figure(1);
linewidth = 3;
plot(x,ymaxlc,x,ymaxmc,x,ymaxcc,x,ymaxhc,x,ymaxpc);
hx = xlabel('Frequency (MHz)');
hy = ylabel('Max Potential (V)');
ht = title('Maximum Potential Transfer at Resonance');
hl = legend('k = 0.1','k = 0.5','k=0.56','k = 0.9', 'k = 1');
set(h,"papersize",[10,10]);
set(hl,"fontsize",12);
set(hx,"fontsize",12);
set(hy,"fontsize",12);
set(ht,"fontsize",20);
set(gca,'XTick',[0:0.5e6:4e6]);
set(gca,"XTickLabel",'0','0.5','1','1.5','2','2.5','3','3.5','4');

% Input values for coupling coefficient for 3D graph of
% sine output with more efficient precision 3D input.
u = [0:0.008:1];
xn = [0:32e3:4000e3];

% Figure 2: 3D sine of max transfer with free coupling k.
hs = figure(2);
[X,Y] = meshgrid(u,xn);
Z = e4max(X,Y);
mesh(X,Y,Z);
hxs = xlabel('Coupling Coefficient k');
hys = ylabel('Frequency (MHz)');
hzs = zlabel('Voltage (V)');
```

```
hts = title('Max Potential at Resonance with Free Coupling');
set(hs,"papersize",[10,10]);
set(hxs,"fontsize",12);
set(hys,"fontsize",12);
set(hzs,"fontsize",12);
set(hts,"fontsize",20);
set(gca,'YTick',[0:1e6:4e6]);
set(gca,"YTickLabel",'0','1','2','3','4');

% Figure 3: Phase of max transfer with free coupling k.
hph = figure(3);
[X,Y] = meshgrid(u,xn);
Z = phase(X,Y);
surf(X,Y,Z);
hxph = xlabel('Coupling Coefficient k');
hyph = ylabel('Frequency (MHz)');
hzph = zlabel('Phase Angle (radians)');
htph = title('Phase of Max Potential at Output');
set(hph,"papersize",[10,10]);
set(hxph,"fontsize",12);
set(hyph,"fontsize",12);
set(hzph,"fontsize",12);
set(htph,"fontsize",20);
set(gca,'YTick',[0:1e6:4e6]);
set(gca,"YTickLabel",'0','1','2','3','4');
```

Appendix C

Data and Figures for Empirical Formulas

FIGURE C.1: American Wire Gauge (AWG) Equivalent Metric Measurements

Gauge (AWG)	CS Area (mm ²)	Gauge (AWG)	CS Area (mm ²)
1	42.4	16	1.31
2	33.6	17	1.04
3	26.7	18	0.823
4	21.1	19	0.653
5	16.8	20	0.518
6	13.3	21	0.410
7	10.5	22	0.326
8	8.36	23	0.258
9	6.63	24	0.205
10	5.26	25	0.162
11	4.17	26	0.129
12	3.31	27	0.102
13	2.62	28	0.0810
14	2.08	29	0.0642
15	1.65	30	0.0509

TABLE C.1: Table of Medhurst Values for Self-Capacitance

l/D Ratio	H value (pF/cm)
50	5.8
40	4.6
30	3.4
25	2.9
20	2.36
15	1.86
10	1.32
9	1.22
8	1.12
7	1.01
6	0.92
5	0.81
4.5	0.77
4	0.72
3.5	0.67
3	0.61
2.5	0.56
2	0.5
1.5	0.47
1	0.46
0.9	0.46
0.8	0.47
0.7	0.47
0.6	0.48
0.5	0.5
0.45	0.52
0.4	0.54
0.36	0.57
0.3	0.6
0.25	0.64
0.2	0.7
0.15	0.79
0.1	0.96

Note: The cubic trendline $f(l/D) = -0.00002(l/D)^3 + 0.0021(l/D)^2 + 0.0546(l/D) + 0.5244$ (correlation $R^2 = 0.9909$) is used for interpolation of data not listed in table D.2 for the sake of our simulation. This trendline is plotted in a diagram on the following page.

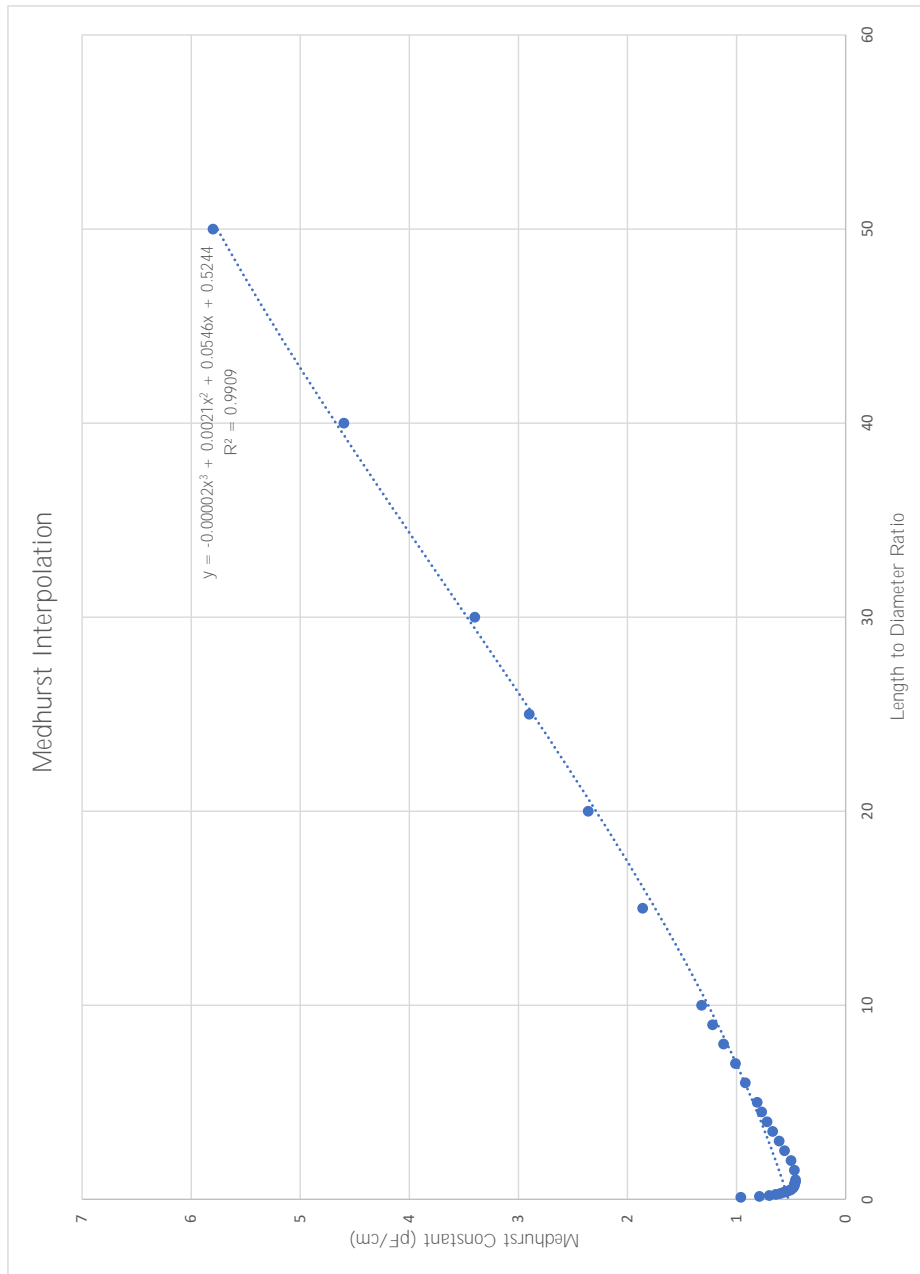


FIGURE C.2: Medhurst interpolation

Appendix D

Detailed Numerical Calculations

Work must now be done to evaluate each of the constants present in equation (4.11). Some of these constants are easier than others, while some require conditions laid out in §4.2.

By using the rudimentary formula for resistance R as related to resistivity ρ , and based on data collected in [1], the medium resistances are calculated here (see Appendix D for conversion from American wire gauge to metric). Note that the skin effect is accounted for in the thicker coils, as described in §3.2.

$$\begin{aligned}
 R_1 = R_4 &\approx \frac{10d_1\rho_{\text{Cu}}}{3\left(2r_1\sqrt{\frac{2\rho_{\text{Cu}}}{\omega\mu_{\text{Cu}}}} - \frac{6\rho_{\text{Cu}}}{\omega\mu_{\text{Cu}}}\right)} \\
 &= \frac{10(0.1986 \text{ m})(1.68 \times 10^{-8} \text{ }\Omega\text{m})}{3\left[0.00326 \text{ m}\sqrt{\frac{2(1.68 \times 10^{-8} \text{ }\Omega\text{m})}{\omega(0.999994)(4\pi \times 10^{-7} \text{ H/m})}} - \frac{6(1.68 \times 10^{-8} \text{ }\Omega\text{m})}{\omega(0.999994)(4\pi \times 10^{-7} \text{ H/m})}\right]} \\
 &= \frac{3.34 \times 10^{-8}}{0.00978\sqrt{\frac{0.0267}{\omega}} - \frac{0.0802}{\omega}} \text{ }\Omega \\
 &= \frac{3.42 \text{ }\Omega}{10^6\left(\sqrt{\frac{0.0267}{\omega}} - \frac{0.0802}{\omega}\right)},
 \end{aligned}$$

$$\begin{aligned}
 R_2 = R_3 &= \rho \frac{l_2}{A_2} = \rho_{\text{Cu}} \cdot \frac{\pi \cdot d_2 \cdot n_2}{A_2} \\
 &= (1.68 \times 10^{-8} \text{ }\Omega\text{m}) \cdot \frac{\pi \cdot 0.0500 \text{ m} \cdot 1,000}{\pi \cdot (30 \text{ awg}/2)^2} \\
 &= (1.68 \times 10^{-8}) \cdot \frac{50}{(0.0001276)^2} \text{ }\Omega \\
 &= 51.6 \text{ }\Omega.
 \end{aligned}$$

A similar evaluation may be done for the inductances of each coil:

$$\begin{aligned}
 L_1 = L_4 &\approx \frac{n_1^2\mu_{\text{Cu}}d_1}{2} \left[\ln\left(\frac{4d_1}{r_1}\right) - 2 \right] \\
 &= \frac{(10^2)(0.999994)(4\pi \times 10^{-7} \text{ H/m})(0.1986 \text{ m})}{2} \left[\ln\left(\frac{4(0.1986 \text{ m})}{(8 \text{ awg}/2)}\right) - 2 \right]
 \end{aligned}$$

$$\begin{aligned}
&= (124.78 \times 10^{-7}) \left[\ln \left(\frac{0.7944}{0.00163} \right) - 2 \right] \text{ H} \\
&= (124.78 \times 10^{-7})(4.189) \text{ H} \\
&= 5.22 \times 10^{-5} \text{ H or } 52.2 \text{ } \mu\text{H},
\end{aligned}$$

$$\begin{aligned}
L_2 = L_3 &\approx \frac{n_2^2 \mu_{\text{Cu}} d_2}{2} \left[\ln \left(\frac{4d_2}{r_2} \right) - 2 \right] \\
&= \frac{(1,000^2)(0.999994)(4\pi \times 10^{-7} \text{ H/m})(0.0500 \text{ m})}{2} \left[\ln \left(\frac{4(0.0500 \text{ m})}{(30 \text{ awg}/2)} \right) - 2 \right] \\
&= (0.03142) \left[\ln \left(\frac{0.200}{0.0001275} \right) - 2 \right] \text{ H} \\
&= (0.03142)(5.358) \text{ H} \\
&= 0.168 \text{ H or } 1.68 \times 10^5 \text{ } \mu\text{H}.
\end{aligned}$$

Using these figures then allow us to calculate the magnetizing values L_m and leakage values L_l for both transmitter and receiver. Letting k be a free value, we obtain the following (recall that $L_1 = L_4$ and $L_2 = L_3$):

$$\begin{aligned}
L_{l1} = L_{l4} &= L_1 - \left(\frac{n_1}{n_2} \right) k \sqrt{L_1 L_2} \\
&= 52.2 - \left(\frac{10}{1,000} \right) k \sqrt{(52.2)(1.68)(10^5)} \text{ } \mu\text{H} \\
&= 52.2 - 29.6k \text{ } \mu\text{H},
\end{aligned}$$

$$\begin{aligned}
L_{l2} = L_{l3} &= L_2 - \left(\frac{n_2}{n_1} \right) k \sqrt{L_1 L_2} \\
&= 1.68 \times 10^5 - \left(\frac{1000}{10} \right) k \sqrt{(52.2)(1.68)(10^5)} \text{ } \mu\text{H} \\
&= (1.68 - 2.96k) \times 10^5 \text{ } \mu\text{H}.
\end{aligned}$$

For the magnetizing inductances,

$$\begin{aligned}
L_{m1} &= \left(\frac{n_1}{n_2} \right) k \sqrt{L_1 L_2} \\
&= \left(\frac{10}{1000} \right) k \sqrt{(52.2)(1.68)(10^5)} \text{ } \mu\text{H} \\
&= 29.6k \text{ } \mu\text{H},
\end{aligned}$$

$$\begin{aligned}
L_{m2} &= \left(\frac{n_2}{n_1} \right) k \sqrt{L_1 L_2} \\
&= \left(\frac{1000}{10} \right) k \sqrt{(52.2)(1.68)(10^5)} \text{ } \mu\text{H} \\
&= 2.96k \times 10^5 \text{ } \mu\text{H}.
\end{aligned}$$

Due to the large coefficient multiplying k , both L_{l2} and L_{l3} will only exhibit non-negative inductance when $k \leq 0.568$. This means that for any coupling that is more efficient,

L_{l2} and L_{l3} will behave similarly to capacitors of an opposite phase to the initial assumption, since the frequency ω is fixed. However, these details remain notable, but somewhat ineffectual, against the mathematical setup of total impedance in both transformer circuits, as this will implicitly manifest in solutions that we find. Nonetheless, it is important to note the repercussions of such a numerical result, especially the fact that the magnetizing inductances L_m , simply by figuring, do not appear to be negligible, and may in fact include numbers for a small parasitic capacitance effect.

For the spherical capacitors C_t and C_r ,

$$\begin{aligned} C_t = C_r &= 4\pi\epsilon_0 r \\ &= 4\pi(8.85 \times 10^{-12} \text{ F/m})(0.06 \text{ m}) \\ &= 6.673 \times 10^{-12} \text{ F or } 6.673 \text{ pF.} \end{aligned}$$

For the parasitic capacitance C_{p1} and C_{p2} using Medhurst's formula (see Appendix A and Appendix D) with a cubic interpolated H value for $l/D = 5.1$,

$$\begin{aligned} C_{p1} = C_{p2} &= H \cdot d_2 \\ &= [-0.00002(5.1)^3 + 0.0021(5.1)^2 + 0.0546(5.1) + 0.5244] \text{ pF/cm} \cdot 5 \text{ cm} \\ &= 4.274 \text{ pF.} \end{aligned}$$

Bibliography

- [1] Derek Marzolf, Byron Okine, Cagatay Mitil, and Andrew Matthews. *Design and Testing of Wireless Energy Transmission*. April 2012.
- [2] Shu Yuen Ron Hui, Wenxing Zhong, and Chi Kwan Lee. A critical review of recent progress in mid-range wireless power transfer. *IEEE Transactions on Power Electronics*, 29(9):4500–4511, 2014.
- [3] James Clark Maxwell. *A Treatise on Electricity and Magnetism*. Dover, 1 edition, 1873.
- [4] A. D. Rawlins. Note on the Capacitance of Two Closely Separate Spheres. *IMA Journal of Applied Mathematics*, 34:119–120, 1985.
- [5] Nikola Tesla. Apparatus for transmitting electrical energy, December 1 1914. US Patent 1,119,732.
- [6] Wenxing Zhong, Chi Kwan Lee, and SY Ron Hui. General analysis on the use of tesla’s resonators in domino forms for wireless power transfer. *IEEE Transactions on Industrial Electronics*, 60(1):261–270, 2013.
- [7] Jiejian Dai and Daniel C Ludois. A survey of wireless power transfer and a critical comparison of inductive and capacitive coupling for small gap applications. *IEEE Transactions on Power Electronics*, 30(11):6017–6029, 2015.
- [8] B. Sacco and A. K. Tomilin. The study of electromagnetic processes in the experiments of Tesla.
- [9] the retarded phase factor in wireless power transmission.
- [10] Xiaodong Liu, Qichang Liang, and Yu Liang. Wireless Power Transmission in Near-Field Range Utilizing Retardation Phase Shift, 2014.
- [11] Qichang Liang, Yu Liang, and Xiaodong Liu. Energy Multiplier in Retarded Resonance.
- [12] Vic Christianto and Florentin Smarandache. A Note on Computer Solution of Wireless Energy Transmission via Magnetic Resonance. 1:81–82, 2008.
- [13] Victor Christianto and Yunita Umniyati. An Exact Solution of a Coupled ODE for Wireless Energy Transmission via Magnetic Resonance. 2014.
- [14] Xun Zhou, Rui Zhang, and Chin Keong Ho. Wireless information and power transfer: Architecture design and rate-energy tradeoff. *IEEE Transactions on Communications*, 61(11):4754–4767, 2013.

-
- [15] Ned Mohan, Tore Undeland, and William P. Robbins. *Power Electronics: Converters, Applications, and Design*. Wiley, 3rd edition, 2007.
- [16] C. P. Steinmetz. *Theory and Calculation of Alternating Current Phenomena*. McGraw Hill, 5th edition, 1916.
- [17] Egon Brenner and Mansour Javid. *Analysis of Electric Circuits*. McGraw-Hill, 2 edition, 1959.
- [18] Kay Hameyer. *Electrical Machines I: Basics, Design, Function, Operation*. RWTH Aachen University Institute of Electrical Machines, 2001.
- [19] William G. Hurley and David J. Wilcox. Calculation of Leakage Inductance in Transformer Windings. *IEEE Transactions in Power Electronics*, 9(1):121–126, January 1994.
- [20] L. Lorenz. Ueber die Fortpflanzung der Electricitat. *Annalen der Physik und Chemie (Annals of Physics and Chemistry)*, 243:161–193, 1879.
- [21] R. G. Medhurst (GEC Research Labs). H.F. Resistance and Self-Capacitance of Single-Layer Solenoids. *Wireless Engineer*, pages 35–43, February 1947. URL <http://www.g3ynh.info/zdocs/refs/Medhurst/Med35-43.pdf>.
- [22] R. G. Medhurst (GEC Research Labs). H.F. Resistance and Self-Capacitance of Single-Layer Solenoids (continuation). *Wireless Engineer*, pages 80–92, March 1947. URL <http://www.g3ynh.info/zdocs/refs/Medhurst/Med80-92.pdf>.
- [23] Harold A. Wheeler. Simple Formulas for Radio Coils. *Proceedings of the Institute of Radio Engineers*, 3(10):1398–1400, October 1928.
- [24] Harold A. Wheeler. Discussion on Simple Inductance Formulas for Radio Coils. *Proceedings of the Institute of Radio Engineers*, 17(3):580–582, March 1929.
- [25] Matthew N. O. Sadiku. *Elements of Electromagnetics*. Oxford University Press, 4th edition, 2007.